ORIGINAL PAPER

A comparative study of ecohydrologies of a tropical mangrove and a broadleaf deciduous forest using eddy covariance measurement

Pramit Kumar Deb Burman[1,2] · Supriyo Chakraborty[1,2] · Tarek S. El-Madany[3] · R. Ramasubramanian[4] · Nirmali Gogoi[5] · Palingamoorthy Gnanamoorthy[4,6] · Charuta Murkute[1] · R. Nagarajan[4] · Anandakumar Karipot[2]

Abstract

Evapotranspiration denotes the transport of water vapor between an ecosystem and atmosphere comprising the biotic (transpiration) and abiotic (evaporation) components. Additionally, the water vapor transports the energy used for its vaporization, the latent heat. In the present study we compare the ecohydrological cycle of a mangrove on the Bay of Bengal coast in southeast India with a broadleaf deciduous forest in northeast India using eddy covariance flux measurement for the very first time. Similar to a semi-arid ecosystem the evapotranspiration from mangrove is dominated by the dry sensible heat flux throughout the year, except pre-monsoon when it behaves like a well-watered ecosystem with evapotranspiration dominating the sensible heat flux. Such behavior is in stark contrast with the broadleaf deciduous forest which provides stronger evapotranspirative heating than sensible heat throughout the year including the dry seasons. The evaporative fraction remains consistently much lower at the mangrove than the broadleaf deciduous forest. Compared to the broadleaf deciduous forest, the mangrove ecosystem remains tighter coupled with the atmosphere. Transpiration contributes the larger share to the evapotranspiration of mangrove even in the dry seasons, whereas transpiration and evaporation contribute maximum to the evapotranspiration of broadleaf deciduous forest periodically through the year. Based on principal component analysis we show that both transpiration and evaporation at the mangrove are most strongly coupled with salinity, much different from the broadleaf deciduous forest where transpiration and evaporation are most tightly coupled with root-zone soil moisture and wind speed, respectively. The salinity regulation of transpiration has an important implication for the carbon cycle of mangrove and its appropriate parameterization in ecosystem and climate models.

✉ Pramit Kumar Deb Burman
  pramit.cat@tropmet.res.in

1   Centre for Climate Change Research, Indian Institute of Tropical Meteorology, Ministry of Earth Sciences, Pune 411008, India

2   Department of Atmospheric and Space Sciences, Savitribai Phule Pune University, Pune 411007, India

3   Max Planck Institute for Biogeochemistry, Jena, Germany

4   Coastal Systems Research, MS Swaminathan Research Foundation, Chennai 600113, India

5   Department of Environmental Sciences, Tezpur University, Tezpur 784028, India

6   Key Laboratory of Tropical Forest Ecology, Xishuangbanna Tropical Botanical Garden, Chinese Academy of Sciences, Menglun, China

1 Introduction

Mangroves are wetland ecosystems found in the coastal area near the confluence of rivers (Donato et al. 2011). These ecosystems not only provide livelihood to the local population through fishery, shrimp farming, firewood and tourism, but also act as natural barriers for dampening the oceanic eddies such as tsunamis, cyclones etc. (Marois and Mitsch 2015) upon their landfall. Apart from such socioeconomic values these also offer high carbon sequestration potential, often larger than the inland 'dry' terrestrial ecosystems, crucial for the climate change mitigation (IPCC 2013a, b; Barros et al. 2014). A large amount of carbon is stored in these partly submerged ecosystems often termed the 'blue carbon' (Alongi 2014).

Located at the juncture of soil, water and atmosphere the hydrology of mangroves is an amalgamation of complex biogeophysical and biogeochemical processes between the plants and environmental variables (Alongi 2014). The trace

gas exchanges of terrestrial ecosystems with atmosphere including CO_2, water vapor and CH_4 are controlled by the environmental variables such as global radiation, air temperature, vapor pressure deficit and soil water content. In addition, for mangroves the water parameters also play crucial roles in such exchanges. Usually growing in the regions with high radiation, evaporative demand and salinity, mangroves experience water-stressed conditions (Passioura et al. 1992; Barr et al. 2014) which make these ecosystems highly efficient in water use and capable of optimizing the carbon gain with minimum water loss (Krauss et al. 2015). Hughes et al. (2001) found the rainfall and tidal flooding to be the primary drivers of ecosystem–atmosphere water vapor exchange at a temperate salt-marsh mangrove in Australia and highlighted the supremacy of in situ measurements over empirical models in studying these phenomena.

In most ecosystem-, weather- and climate models terrestrial ecosystems are specified as different plant functional types (Hughes et al. 2001) and their atmospheric trace gas exchanges are calculated based on the empirically derived functional relations among measured trace gas concentrations, environmental variables and plant-physiological parameters. The magnitude, pattern and physiological and environmental drivers of atmospheric exchanges of trace gases and energy of the mangrove ecosystems are much different from the dry terrestrial ecosystems. Hence the mangroves are poised to respond to climate change in a much different way from the terrestrial ecosystems. However, due to the sparsity of measurements to precisely decipher such relations among the fluxes and their governing variables the mangroves remain poorly represented in such models (Berger et al. 2008; Verheijen et al. 2015) which is also presently a key area of uncertainty in projecting the impact of climate change on mangrove ecosystems.

In fact, in several of these models no dedicated PFT for mangrove is found which is partially due to the lack of clear consensus in the scientific community whether to treat these ecosystems as wetlands or forests (IPCC 2013a, b; Bongaarts 2019). Thus, uncertainty arises in upscaling the measured ecosystem-level trace gas fluxes from the mangroves to the regional and global scales (Luo et al. 2010). To address this problem, it is necessary to comparatively assess the biosphere–atmosphere exchanges of trace gases and energies at mangroves and dry inland ecosystems and highlight the similarities and differences to be implemented in the aforementioned models.

In a warmer environment induced by climate change these processes are slated to behave in much different ways posing a threat to the existence and biodiversity of mangroves (Luo et al. 2010). For proper mitigation measures such processes need to be efficiently represented in process-based ecosystem-, Earth system- and climate models which presently remain largely unknown. The long coastline of India along the Bay of Bengal and Arabian Sea houses a significant patch of mangroves distributed over several locations (Giri et al. 2015). The Sundarban Biosphere Reserve, a contiguous mangrove in the Gangetic delta shared between India and Bangladesh is the largest mangrove ecosystem in the world. According to the latest national forest report, mangroves occupy 4975 km^2 area in the Indian landmass accounting for 0.70% of the total forest cover of India (India State of Forest Report 2019).

Several of the Indian mangroves are located in densely populated regions and exposed to the severe threat of rapid land-cover and land-use change driven by the agricultural expansion for their offering of fertile soil in less saline fringe regions (Datta and Deb 2012; Singh et al. 2014). Several observational and satellite-based studies have investigated various aspects of these mangroves and mapped the extent and health of these mangroves at Sundarban (Akhand et al. 2016), Coringa (Satapathy et al. 2007), Pichavaram, Bhitarkanika (Chauhan et al. 2008), Muthupet (Krithika et al. 2008; Kripa et al. 2019), etc. Forest biomass, salinity pattern, greenhouse gas emissions from soil have been documented by slow chamber-based methods (Purvaja et al. 2004; Gnanamoorthy et al. 2019). However, the high-frequency eddy covariance (EC) technique offers an unprecedented advantage in the proper estimation of evapotranspiration over the other modes of measurement (Baldocchi 2003) which is still sparse in the Indian mangroves (Rodda et al. 2016). Additionally, the partitioning of evapotranspiration into its components measured using the EC method remains challenging. In fact, to the best of our knowledge no study exists for assessing the evaporation and transpiration separately for the mangroves in the Indian subcontinent. Subsequently, the role of environmental drivers (including salinity) on transpiration and evaporation also remain largely unknown. To be specific, such underrepresentation of the mangrove ecosystems is one of the key sources of uncertainty in modelling the impact of climate change on the biomes in the south Asian region as highlighted by Kumar and Scheiter (2019).

To bridge this gap the MetFlux India project endeavors to gather EC-based observational data at a few natural ecosystems in India (Deb Burman et al. 2017; Deb Burman et al. (2020b), Chakraborty et al. 2020). As part of this network several instrumented micrometeorological flux towers have been installed, aimed at the continuous monitoring of energy and greenhouse gas fluxes from the terrestrial ecosystems in India (Deb Burman et al. 2020a). In our present comparative study we address this problem by using the MetFlux India observations from a mangrove and a broadleaf deciduous forest to bring out the differences in evapotranspiration, their components and drivers at these two ecosystem types in India.

The objectives of this paper were threefold. First, we want to study how strong is the evapotranspirative forcing by a

tropical mangrove ecosystem in comparison with a tropical broadleaf deciduous forest to the atmosphere. Second, we want to compare their annual evapotranspiration patterns and quantify the relative contributions of evaporation and transpiration in the same for both the ecosystems. Finally, we want to find out the major controlling factors of evaporation and transpiration for these different types of ecosystems.

2 Materials and methods

2.1 Study sites

The Pichavaram Mangroves (PVM) are situated on the southeast coast of India in Tamil Nadu along the Bay of Bengal on the Cauvery delta between Coleroon and Vellar estuaries (11.22°–11.30° N, 79.49°–51.24° E). According to Gnanappazham and Selvam (2014) the tidal flats and mudflats without vegetation occupy 660 ha and the tidal flats

with mangrove occupy 858 ha in this mangrove. A 10 m-tall micrometeorological flux tower equipped with EC setup and other associated meteorological and soil measurement sensors at multiple heights and depths for continuous measurements of scalar and energy fluxes was erected by the Indian Institute of Tropical Meteorology, Pune, in collaboration with the MS Swaminathan Research Foundation, Chennai in this ecosystem (11.43° N, 79.79° E) as part of the MetFlux India network (Fig. 1). The mangrove vegetation surrounding this tower has an average height of 3 m and comprises mostly *Avicennia marina* along with *Rhizophora* spp whose average leaf area index (LAI) varies approximately between 1.2 and 3.5 $m^2\,m^{-2}$ annually as found from the in situ measurements using a portable sensor (LAI2200, Li-COR Biosciences, Lincoln, USA) (Gnanamoorthy et al. 2019). The PVM flux tower has an average measurement footprint radius of 206 m, and more details regarding its instrumentation can be found in Gnanamoorthy et al. (2020).
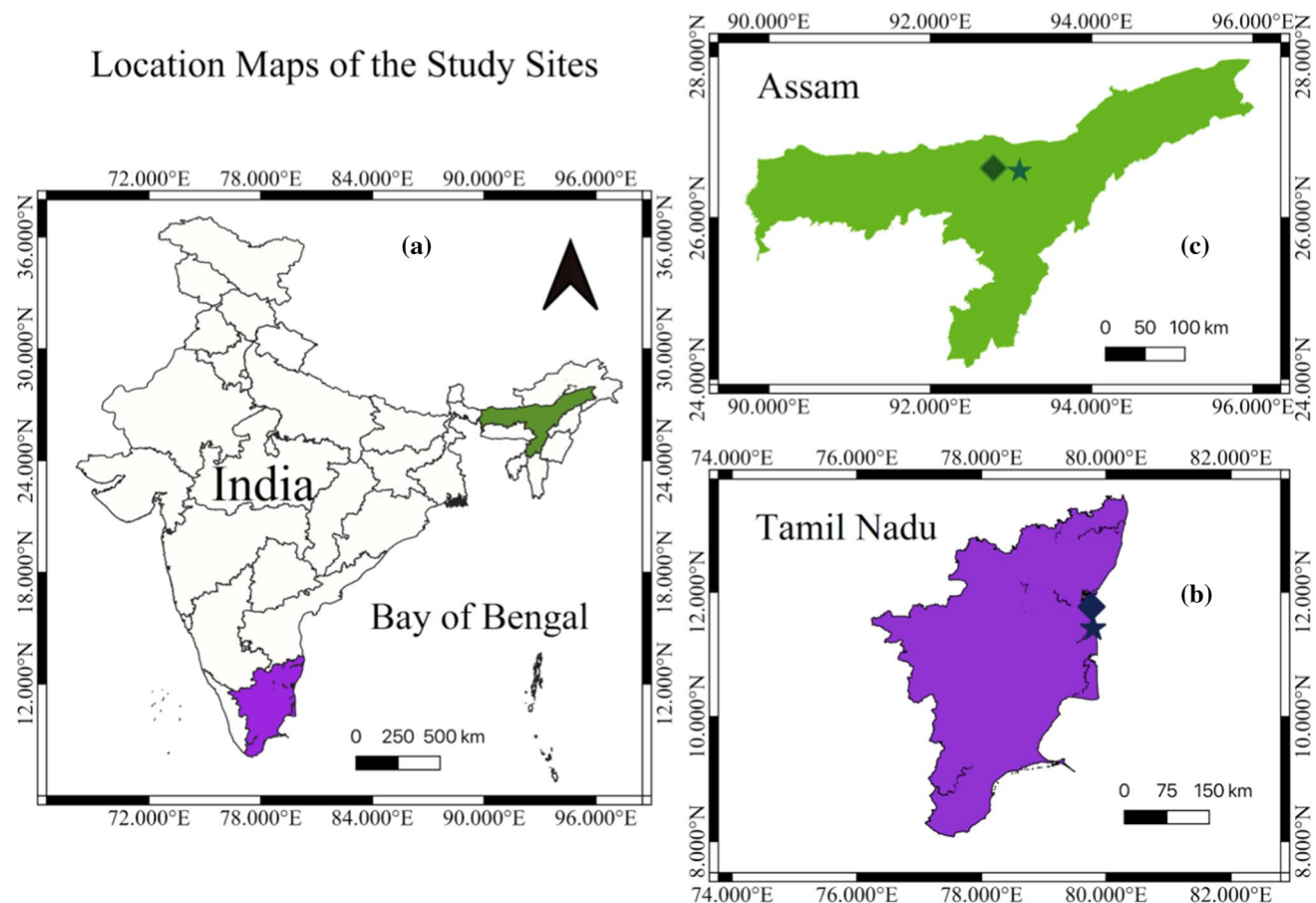
Fig. 1 Geographical locations of the study sites (anticlockwise from left); **a** the states of Tamil Nadu and Assam are highlighted on the map of India in purple and green, respectively, with the arrow pointing towards the north direction, **b** Pichavaram flux tower (PVM) and Cuddalore surface observatory by the India Meteorological Department (IMD) are marked on the map of Tamil Nadu with star and diamond symbols, respectively, and **c** Kaziranga National Park (KNP) flux tower and Tezpur surface observatory by the India Meteorological Department (IMD) is marked on the map of India with star and diamond symbols respectively

Every month the water salinity (ST) was measured in situ at 0.3 m depth at eight places surrounding the PVM flux tower using the multiprobe water quality monitoring system (Hydrolab Quanta, Austin, Texas, USA). This system was calibrated every month using standard solutions in the laboratory. The ST measurements are subsequently averaged over these measurement locations each month since the temporal variation of this parameter is satisfactorily captured at this temporal scale (Boyer and Levitus 2002; Das et al. 2017). This mangrove ecosystem is less influenced by tidal activities and classified as river-dominated (Selvam 2003). The Uppanar, a tributary of the Coleroon River in the south and the Vellar estuary in the north of the PVM region are rainfed.

The Kaziranga National Park (KNP) is a moist evergreen, semi-deciduous forest in the state of Assam in northeast India, the region with maximum forest coverage (India State of Forest Report 2019) in the country. As part of the MetFlux India network a 50 m-tall flux tower with EC setup and other associated meteorological and soil measurements at multiple heights and depths was erected in this forest (26.58° N, 93.1° E) surrounded by vegetation with an average canopy height of 20 m (Fig. 1). *Gmelina arborea* Roxb., *Mallotus repandas* (willd) Müll. Arg*., Tetrameles nudiflora* R. Br. are among the major plant species found around the site. The KNP flux tower has an average measurement footprint radius of 400 m (Deb Burman et al. 2020a). The details on its instrumentation and surrounding floristic composition can be found in Deb Burman et al. (2019) and Sarma et al. (2019), respectively. The annual LAI varies approximately within 0.75–3.25 $m^2 m^{-2}$, as found from the in situ measurements (Deb Burman et al. 2017). The geographical locations of PVM and KNP flux towers are shown in Fig. 1.

2.2 Site climate

According to the Köppen-Geiger climate classification (Beck et al. 2018), the local climates in PVM and KNP are identified as tropical savannah (Aw) and humid subtropical (CWa) types, respectively. The air temperature and precipitation climatology for both the sites are calculated as the monthly mean of 30 years measurement during 1981–2010 at the nearest available surface observatories at Cuddalore (11.46° N, 79.46° E) and Tezpur (26.62° N, 92.78° E), respectively, maintained by the India Meteorological Department (IMD) (Fig. 1) (Jaswal et al. 2014; Suresh and Bhatnagar 2005) and plotted in Fig. 2.

2.3 In situ data

For our analysis we have used the latent heat flux (LE in W m^{-2}) as the measure of evapotranspiration (ET) in the energy flux unit during an 11-month period from October 2017 to August 2018 at PVM and the year of 2016 at KNP. Additionally, the sensible heat flux (H in W m^{-2}), net radiation (R_n in W m^{-2}), incoming shortwave radiation (R_g in W m^{-2}; interchangeably known as the global radiation), air temperature (T_{air} in °C), air pressure (P_{air} in hPa), precipitation (P_n in mm) and horizontal wind speed (WS in m s^{-1}) have been used for the analyses during the corresponding measurement periods at each site.

2.3.1 Measured data records

At both the sites, LE and H are calculated from the high frequency EC measurements over the canopy, at 10 m at PVM and 37 m at KNP. Each EC setup includes a 3D sonic anemometer-thermometer (WindMaster Pro, Gill Instruments, Lymington, UK) and an enclosed path CO_2 and H_2O infrared gas analyzer (LI7200, Li-COR Biosciences, Lincoln, USA). The R_n is recorded as the resultant of incoming and outgoing shortwave and longwave radiations every 30-min by the four-component net radiometers (NR01, Hukseflux, Manorville, NY, USA) installed at 6 m at PVM and 19 m at KNP. The multi-component weather sensors (WXT520, Vaisala Oyj., Vantaa, Finland) record T_{air}, P_{air}, P_n and WS every 30-min at 10 and 37 m at PVM and KNP, respectively.

2.3.2 Data processing

The raw EC measurements are quality-controlled according to a set of recommended pre-processing recipes (Aubinet et al. 2012) before calculating the Reynolds averaged half-hourly fluxes in EddyPro software version 6.2.0 (https://www.licor.com). These half-hourly fluxes are further checked for outliers and erroneous values are removed. The vapor pressure deficit (VPD in hPa) is calculated from T_{air} and relative humidity (RH in %) measurements by the WXT520 weather sensors (Campbell and Norman 1998). The meteorological variables are quality-controlled following Papale et al. (2006). This set of data include only the measured values and have been used in the analyses of the present paper without any gap-filling i.e. the data with best quality flag 0 (Mauder and Foken 2004). All the above-mentioned data handling operations are detailed in Gnanamoorthy et al. (2019) for PVM and Deb Burman et al. (2019) for KNP. The monthly-averaged values of T_{air} and monthly total values of P_n are calculated from their complete half-hourly values for comparing with the climatological records at the corresponding sites.

2.3.3 GLEAM data

For the present analysis the water content in soil at KNP is taken from the Global Land Evaporation Amsterdam Model (GLEAM) (Miralles et al. 2011), which is a globally
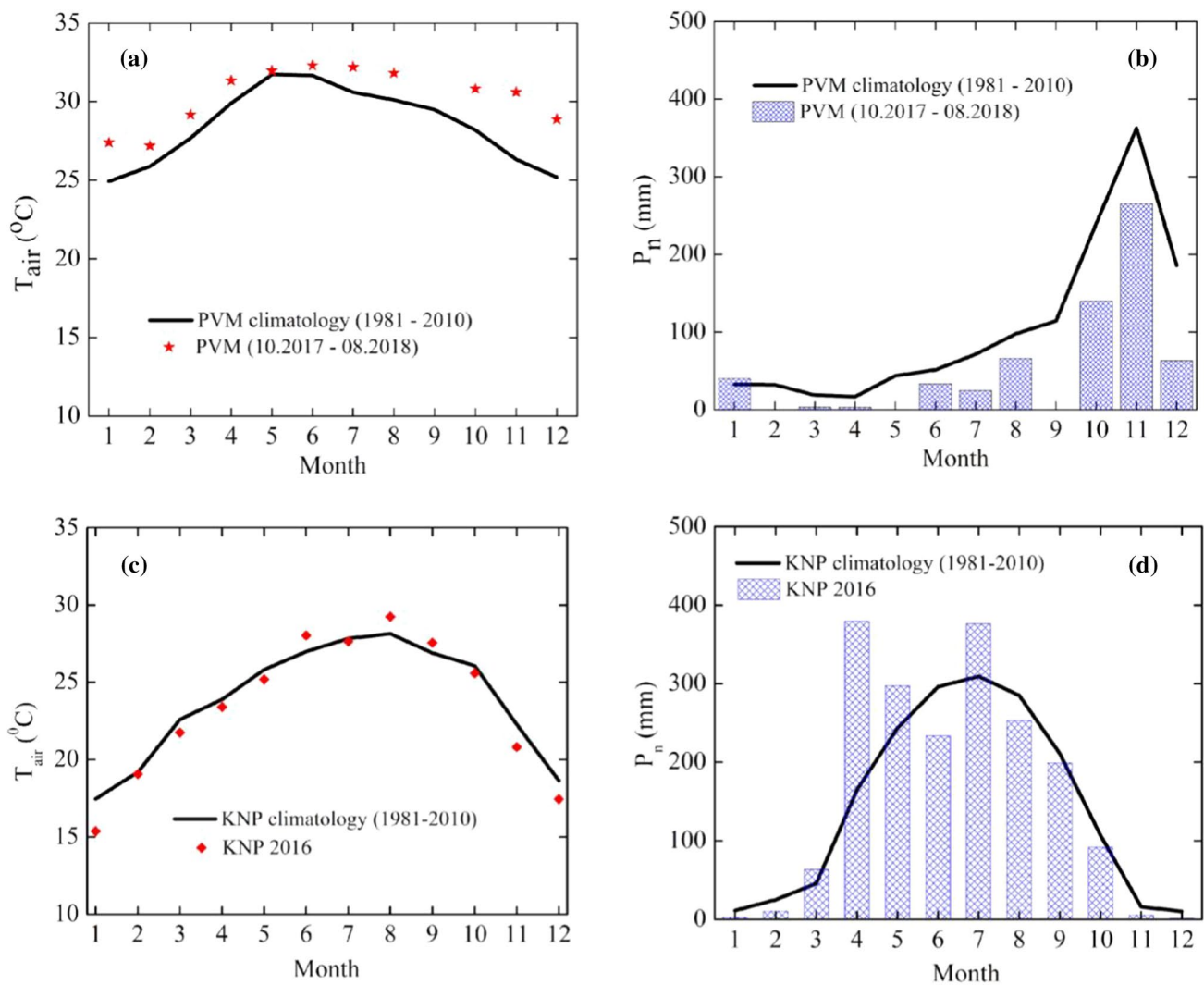
Fig. 2 Climatological and measured monthly averaged **a** air temperature (T_{air}), **b** precipitation (P_n) at Pichavaram Mangroves (PVM), **c** T_{air}, and **d** P_n at Kaziranga National Park (KNP). Corresponding measurement durations are provided in the parentheses in the figure

modeled daily land evaporation product primarily derived from the satellite measurements based on the Priestley & Taylor formulation (Priestley and Taylor 1972) and validated against multiple EC measurements sites across the globe.

As inputs to this model the soil water content and vegetation optical depth remotely sensed using the microwave band are used along with the surface radiation and near-surface air temperature from reanalysis data and rainfall and snowmelt components from multi-source ensemble products. Additionally, the running water budget components are corrected every day using the Kalman filter assimilation (Crow 2007) to account for the uncertainties in satellite measurements. The details about this methodology can be found in Miralles et al. (2011) and Martens et al. (2017).

In the GLEAM methodology two types of soil water content are produced in the units of volumetric ratio. These are namely the surface soil moisture and root-zone soil moisture

in $m^3\ m^{-3}$. The surface soil moisture (SM) represents the water content in the topsoil layer, confined till 0.10 m depth from the soil surface. For the bare soil, this effectively contributes to the evaporation. However, any vegetation canopy can access the water content much deeper within the soil due to the penetration of roots which is termed as the root-zone soil moisture (RM). For tall forest canopies such as KNP the RM is integrated over the depths from 0.05 m to 2.50 m (Miralles et al. 2011).

Version 3.3a of the GLEAM data (hereafter GLEAMv3.3a) is available globally at a spatial resolution of $0.25° \times 0.25°$ for a 39-year time-period from 1980 to 2018 (Martens et al. 2017). In the present work we have computed the area averages of SM and RM from GLEAMv3.3a over a spatial domain extending from 25° to 27° N and 92° to 94° E, surrounding the location of KNP flux-tower. Subsequently we computed the monthly averages of these spatially

averaged SM and RM during 1981–2010 to be used as their climatology at KNP. Additionally, the monthly average values of SM and RM during 2016 at KNP are also used in our analysis.

2.3.4 Evapotranspiration partitioning

Several methods exist for partitioning the evapotranspiration (ET) by an ecosystem into its constituent fluxes, namely evaporation and transpiration (Kool et al. 2014; Stoy et al. 2019). Evaporation (E) is an abiotic physical process that represents the water loss by bare soil and waterbodies, whereas transpiration (T) is a biotic process that regulates the water loss by plants through stomata (Wang and Dickinson 2012). Transpiration is also closely coupled with the photosynthetic CO_2 uptake by plants as both these processes are controlled by the stomatal opening and closure (Bonan 2015). In the present work we have not accounted for the canopy-intercepted water evaporation which is usually the smallest component of ET (Roth et al. 2007). This component is considerably large for coniferous (Bréda et al. 2006) and dense canopies with large LAI (Aussenac 2000). The forest types at PVM and KNP are mangrove and deciduous, respectively, with annually maximum LAI values of 3.5 m^2 m^{-2} (Gnanamoorthy et al. 2019) and 3.25 m^2 m^{-2} (Deb Burman et al. 2017) correspondingly. Hence it is justifiable not to include this flux in our analyses.

We have partitioned ET into E and T in this paper using the open source Fluxpart module (Skaggs et al. 2018) available for the Python 3 programming language (van Rossum and Drake 2009). This code computes E and T separately from the raw EC measurements of wind velocity components, T_{air}, P_{air}, atmospheric water vapor (q in g kg^{-1}) and CO_2 concentrations (c in ppm) using the flux variance similarity method (Scanlon and Sahu 2008; Scanlon and Kustas 2010, 2012) which has been shown to perform well in partitioning the evapotranspiration of forest ecosystems by several researchers (Sulman et al. 2016; Nelson et al. 2020). Before calculating the fluxes the same set of corrections are applied to the high-frequency measurement records for filtering the erroneous values as described in 2.3.2. We have used the 'daytime' partitioning method where the fluxes before sunrise and after sunset are considered as non-stomatal and as perturbations to the correlation between the stomatal CO_2 and water vapor fluxes which forms the basis of the flux variance similarity method (Skaggs et al. 2018). It is to be noted here that the flux-variance similarity method is not well-suited for non-convective conditions (Laubach and Kellihar, 2004). Such conditions however, arose mostly during nighttime during which the ET and its components were negligible. Additionally the advection may corrupt the flux-variance similarity relationships while not contributing significantly towards the fluxes (Mukherjee et al. 2015). Such effects are reflected as large-scale eddies and progressively removed using the wavelet decomposition technique (Skaggs et al. 2018).

The micrometeorological flux-gradient methods work best in the experimental conditions where the source-area of the measured tracer (water vapor, in our case) is homogeneous and near-infinite in nature (Laubach and Kellihar (2004), McMillan et al. (2014)). This condition is satisfied at both our experimental sites i.e. Pichavaram and KNP, where the flux-footprint of the EC towers are large and homogeneous in terms of the terrain and canopy types (Deb Burman et al. 2020a; Gnanamoorthy et al. 2020).

In the absence of separate measurements of evaporation and transpiration, we estimated the leaf-level water use efficiencies (WUEs) of our studied ecosystems from c and q as follows according to Skaggs et al. (2018), at every half an hour during the runtime of flux-partitioning using Fluxpart:

$$WUE = (1/1.6) \times (c_a - c_i)/(q_a - q_i),$$

where c_a and q_a are the ambient values of c and q, and c_i and q_i are intercellular values of c and q, respectively.

Divergent opinions exist on the effect of VPD on the WUE of an ecosystem which is manifested in the functional dependence of c_i/c_a on VPD. We have considered the following four such scenarios, as reported to be mostly followed in the natural ecosystems, in our work and partitioned the evapotranspiration into evaporation and transpiration for each of these:

1. Constant: $c_i/c_a = K$, where $K = 0.7$ for C3 plants

2. Linear: $c_i/c_a = b - m \times$ VPD, where $b \sim 1$ and $m = 0.000164$ Pa^{-1} for C3 plants (Morison and Gifford 1983)

3. Optimized: c_i/c_a is determined followed the optimization model by Scanlon et al. (2019)

and 4. Square-root: $c_i/c_a = 1 - (1.6 \times$ lambd $\times$ VPD) with lambd being 22e−9 kg CO_2 m^{-3} Pa^{-1} (Katul et al. 2009)

At both KNP and PVM the dominant vegetation type is C3 (Metya et al., 2021), as described in Sect. 2.1. Additionally, Deb Burman et al. (2021) reported that at KNP, the daytime c_i/c_a remains constant at ∼ 0.7. Hence, we have chosen this scenario to represent the partitioned fluxes at KNP in our study and to maintain uniformity in analysis followed the same for our other study location at PVM. Further we have calculated the standard errors for evaporation and transpiration computed for the four different scenarios as listed above and used those as the error estimates (Fig. S1). All these methods are found to agree well with each other in determining the magnitudes and patterns of evaporation and transpiration.

2.3.5 Potential evapotranspiration

Potential evapotranspiration (PET) is a measure of the theoretical maximum evapotranspiration from any ecosystem under optimal conditions and no water or nutrient stress (Monteith et al. 1965). It is often used as a measure of the response of the canopy to the atmospheric water demand. Several formulations exist in the literature to compute the same. However, in the present work we have computed the PET following the Penman–Monteith formulation (Allen et al. 1998), recommended as the preferable method for the tropical and subtropical regions (Fisher et al. 2011).

We have represented PET in energy flux unit (W m^{-2}) for easier comparison with the actual transpiration (AET) which is represented in the same convention as LE in the present work. The surface energy budget is closed at 61% and 70% at PVM (Gnanamoorthy et al. 2020) and KNP (Deb Burman et al. 2019), respectively, which match well with the closure obtained at the flux measurement stations (Wilson et al. 2002) and recognized as acceptable degree of closure globally. With this closure no additional correction to the energy fluxes and PET is implemented as recommended by Maes et al. (2019). Additionally, we have computed the evaporative fraction (EF) that is defined as the ratio of LE to R_n (Gentine et al. 2007). It is a measure of the amount of net available energy channelized into the moist latent by any ecosystem.

2.3.6 Atmospheric conductances

The exchanges of mass, energy and momentum between any vegetated land surface and boundary layer of atmosphere can be expressed in terms of several conductances following the flux-gradient analogy (Verma 1987). In the present work, we have computed the aerodynamic (G_a in m s^{-1}) and boundary layer (G_b in m s^{-1}) conductances to water vapor transfer following Thom (1972); Verma (1987) and Hicks et al. (1987) in the Bigleaf analogy in which the entire ecosystem is considered to behave like a single big leaf and individual leaf-level details are averaged at a larger scale to obtain their ecosystem-level counterparts (Sellers 1987). Surface layer conductance to water vapor (G_s in m s^{-1}) is computed inverting the Penman–Monteith equation (Knauer et al. 2018). This approach is particularly useful to parameterize the ecosystem-atmosphere interactions in process-based ecosystem, Earth system and climate change models for their improved performance at a reduced complicacy (Sellers 1997; Dai et al. 2004).

2.3.7 Canopy-atmosphere decoupling coefficient

The concept of a dimensionless coefficient of decoupling between the ecosystem and atmosphere, known as the canopy-atmosphere decoupling coefficient (Ω), was formulated (Jarvis and Mcnaughton 1986) to assess the relative controls of physiology and environment on the water vapor exchange between these two. Lower and higher values of Ω signify stronger and weaker physiological control on the canopy-atmosphere water vapor exchange and termed as tightly and weakly coupled conditions, respectively. For the calculations of PET, conductances and Ω we have used the open-source 'bigleaf' R-package by Knauer et al. (2018).

2.3.8 Principal component analysis

Principal Component Analysis (PCA) is a multi-variate data analysis technique to visualize the inherent variations of a dataset in a more apprehensive way (Jollife and Cadima 2016). In this technique the dimensionality of any dataset (D) is reduced by the eigenvalue decomposition of the covariance matrix (V) of this dataset so that the dataset is reoriented along with the directions with gradually decreasing order of variance explained in the original data D (Hand et al. 2001). The first principal component (PC1) refers to the eigenvector corresponding to the largest eigenvalue of the covariance matrix V which is also the direction with maximum variance. The second principal component (PC2) stands for the eigenvector corresponding to the next largest eigenvector of V and is aligned with the direction with second maximum variance and orthogonal to PC1. Similarly, the nth principal component (PCn) ranks n in terms of explaining the variance while remaining orthogonal to the rest of the principal components.

In this work we have carried out the PCA using the 'prcomp' command in R programming language (R Development Core Team 2011). It uses a robust methodology based on the singular value decomposition (SVD) technique to compute the PCs (Mair 2018); for details about SVD and PCA see Mardia et al. (1997) and Jolliffe (2002). The controls of T_{air}, P_{air}, P_n, WS, VPD, SM, RM and R_n on E and T have been found using PCA at monthly scale at KNP. In addition to these variables the ST has also been included in the PCA for PVM. The monthly scale has been chosen to have a uniform scale still maintaining the maximum possible temporal resolution across all the variables. For all the variables monthly averaged values are computed from their half-hourly measurements except ST, for which a rigorous spatio-temporal averaging removes the outliers and makes the input variables statistically robust by reducing the noise (Ivanov and Evtimov 2014). Finally in our analysis PCA is performed over 11 measurements of 8 variables at PVM and 12 measurements of 7 variables at KNP and thus the probability of misinterpreting the PCA results is eliminated as the number of observations are more than the number of variables in both the cases (Jollife and Cadima 2016).

All the variables have been centered by removing their means and scaled by their respective variances before performing the PCA. Such transformations do not alter the conclusion but improve the visualization of the output (Jollife and Cadima 2016). The standard deviation (σ), proportion of variance (α) and cumulative proportion of variance (γ) of the PCs are listed in Table 1. The biplot is a dual display of the original data along with the projections of the data on PC1 and PC2 on x and y-axes, respectively (Gabriel 1971; Aitchison and Greenacre 2002). On a biplot all the variables are marked with arrows with the length of each

arrow denoting the standard deviation of the variable. The correlation coefficient between any two variables is represented by the cosine of angle between the corresponding arrows (Ivanov and Evtimov 2014). Similarly, the cosine of angle between any variable arrow and x-axis (y-axis) denotes the correlation of that variable with PC1 (PC2); acute and obtuse angles stand for positive and negative correlations, respectively, whereas right angle signifies lack of any correlation (see Table 2).

Table 1 Variables and parameters used in the present study listed in alphabetical order

Symbol	Definition	Unit
AET	Actual evapotranspiration	ppm
C_p	Specific heat of air at constant pressure	J kg^{-1} K^{-1}
c	Atmospheric CO_2 concentration	ppm
d	Displacement height	m
E	Evaporation	W m^{-2}
E_{av}	Quarterly averaged diurnal E	W m^{-2}
EF	Evaporative fraction	–
ET	Evapotranspiration	W m^{-2}
GPP	Gross primary productivity	μmol m^{-2} s^{-1}
GPP_d	Daily GPP	gC m^{-2} d^{-1}
GPP_y	Annual GPP	gC m^{-2} y^{-1}
G_{ac}	Aerodynamic conductance for CO_2 transfer	m s^{-1}
G_{aq}	Aerodynamic conductance for water vapor transfer	m s^{-1}
G_{bc}	Canopy boundary layer conductance for CO_2 transfer	m s^{-1}
H	Sensible heat flux	W m^{-2}
H_{av}	Quarterly averaged diurnal H	W m^{-2}
H_{max}	Maximum value of H_{av}	W m^{-2}
LAI	Leaf area index	m^2 m^{-2}
LE	Latent heat flux	W m^{-2}
LE_{av}	Quarterly averaged diurnal LE	W m^{-2}
LE_{max}	Maximum value of LE_{av}	W m^{-2}
Ω	Canopy–atmosphere decoupling coefficient	–
NEE	Net ecosystem exchange	μmol m^{-2} s^{-1}
P_{air}	Air pressure	hPa
PET	Potential evapotranspiration	W m^{-2}
P_n	Precipitation	mm
q	Atmospheric water vapor concentration	g kg^{-1}
R_g	Incoming shortwave radiation (also known as the global radiation)	W m^{-2}
RH	Relative humidity	%
RM	Root-zone soil moisture	m^3 m^{-3}
R_n	Net radiation	W m^{-2}
SM	Surface soil moisture	m^3 m^{-3}
ST	Salinity	ppt
T	Transpiration	W m^{-2}
T_{air}	Air temperature	°C
T_{av}	Quarterly averaged diurnal T	W m^{-2}
VPD	Vapor pressure deficit	hPa
WS	Horizontal wind speed	m s^{-1}

Table 2 The standard deviation (σ), percentage of variance explained (α), and cumulative percentage of variance explained (γ) by the nth principal component (PCn) from the principal component analyses of transpiration (T) and evaporation (E) at Pichavaram Mangroves (PVM) and Kaziranga National Park (KNP)

	PC1	PC2	PC3	PC4	PC5	PC6	PC7	PC8
T(PVM)								
σ	1.90	1.69	0.86	0.71	0.41	0.38	0.15	0.07
α (%)	45.24	35.89	9.14	6.36	2.08	0.96	0.28	0.06
γ (%)	45.24	81.13	90.26	96.62	98.71	99.66	99.94	100
E (PVM)								
σ	1.82	1.67	0.99	0.85	0.33	0.26	0.16	0.10
α (%)	41.52	34.66	12.21	8.95	1.36	0.87	0.31	0.12
γ (%)	41.52	76.19	88.40	97.35	98.70	99.57	99.89	100
T (KNP)								
σ	2.14	1.48	0.79	0.62	0.38	0.22	0.16	0.07
α (%)	57.17	27.51	7.70	4.82	1.80	0.62	0.33	0.06
γ (%)	57.17	84.68	92.38	97.20	98.99	99.62	99.95	100
E (KNP)								
σ	2.19	1.51	0.64	0.47	0.40	0.33	0.14	0.04
α (%)	60.13	28.46	5.07	2.78	2.00	1.32	0.25	0.02
γ (%)	60.13	88.59	98.36	96.44	98.42	99.74	99.98	100

3 Results and discussion

3.1 Meteorological features of the study sites

Being located closer to the tropics the climate at PVM is warmer as compared to KNP. Climatologically, May and January are the warmest and coldest months at PVM with the monthly mean T_{air} being approximately 32 and 25 °C, respectively (Fig. 2a), whereas November and April are the wettest and driest months with cumulative P_n being approximately 362 and 17 mm correspondingly (Fig. 2b). The climatological annual cumulative P_n at PVM is 1267 mm. On the other hand, the climatologically warmest and coldest months at KNP are August and January with the monthly mean T_{air} being approximately 28 and 17 °C, respectively (Fig. 2c), whereas July and January are the wettest and driest months with cumulative P_n approximately being 300 and 10 mm correspondingly (Fig. 2d). The climatological annual cumulative P_n at KNP is 1725 mm. As it is seen, despite having an inland location, climatologically KNP is wetter than its coastal counterpart PVM.

The annual precipitation pattern at PVM is markedly different from most parts of the mainland peninsular India. Most of this landmass receives maximum precipitation in the summer months (i.e. June–September), during the Indian summer monsoon (also known as the southwest monsoon) (Parthasarathy 1984; Rajeevan et al. 2010), a planetary-scale event characteristic of this region. This includes the upstream region of Cauvery basin in Karnataka that receives rainfall during the southwest monsoon season (June–September) (Gnanappazham and Selvam 2014). However, these months are usually drier at the PVM estuarine area which receives the maximum precipitation in the colder months of October, November and December (Gnanappazham and Selvam 2014). Accordingly, locally the seasons are defined as follows: in contrast to the larger part of the peninsular India, January to March as post-monsoon, April–June as summer, July to September as pre-monsoon and October to December as monsoon (Kathiresan 2000). Apparently, no season is designated as winter in this region.

Climatologically the wettest period at KNP is the summer months from June to September. Additionally, it receives a significant amount of rainfall during April and May due to the thunderstorm activities (Mahanta et al. 2013). The seasons are defined at KNP as follows: December–February as winter, March–May as pre-monsoon, June to September as monsoon and October–November as post-monsoon (Jain and Kumar, 2012).

In our measurement period, compared to the climatic normals all the months are warmer at PVM (Fig. 2a), whereas all the months except January are drier (Fig. 2b). This warming pattern is more prominent (> 4 °C) in November and December. These months are climatologically colder with average T_{air} of 26 and 25 °C, respectively, but in the measurement period record 31 and 29 °C correspondingly. In the analysis period October, November and December receive 140, 265 and 63 mm P_n as compared to the climatological values of 240, 362 and 185 mm, respectively (Fig. 2c). Hence although the annual trends in both T_{air} and P_n follow their climatological patterns at PVM, a drastic desiccation pattern is seen driving the local climate to be warmer and drier.

In contrast to PVM, at KNP no significant change in T_{air} is observed. Here during the analysis period, June and August are warmer than climatology whereas January and December

are colder (Fig. 2c). However, the T_{air} shift remains less than 2 °C and the annual mean T_{air} in the analysis period does not deviate from its climatological value of 23 °C. On the other hand, April, May and July receive more rainfall in the analysis period (P_n is 379, 297 and 376 mm, respectively) as compared to their climatological mean values (165, 244 and 309 mm, respectively) at KNP. However, June and August remain drier (P_n is 233 and 253, respectively, as compared to 296 and 285 mm correspondingly) compared to climatology. Overall, at KNP the cumulative annual P_n is 1915 mm in the measurement period, compared to its climatological value of 1725 mm. Hence, the climate at KNP does not warm up but tends to get wetter.

The monthly total P_n and average ST at PVM are plotted together in Fig. 3. Overall, ST decreases with P_n. Annually maximum ST observed is 41.3 ppt, in the month of May at the end of the dry period when P_n is almost nil (Fig. 3). In the post-monsoon and summer seasons the monthly ST remains higher than 30 ppt except in January when ST is 24 ppt (Fig. 3). During the pre-monsoon and monsoon the ST remains lower than 20 ppt; during August the annual minimum ST of 1.3 ppt is reached (Fig. 3). As explained earlier the upstream region of Cauvery basin receives heavy rainfall every year during the southwest monsoon season (June–September), and as a result a large volume of floodwater flows from this region to the downstream PVM estuary. The volume of this freshwater flow is usually high during the northeast monsoon season (October–December) at PVM (Gnanappazham and Selvam 2014). Additionally in 2018, due to the surplus rainfall in June in Karnataka (Sreejith et al. 2018) a large volume of freshwater was released from the dams in Karnataka from July onwards which resulted in this drop of ST in August at the PVM estuary.
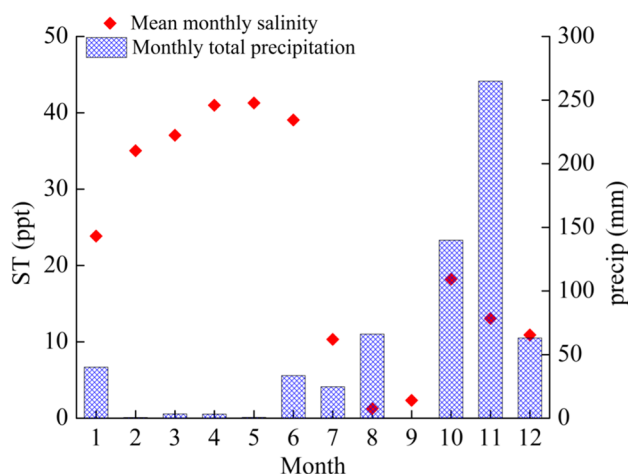
Hence, according to the salinity classification (Barik et al. 2018) the PVM ecosystem swings between a high-saline zone in post-monsoon and summer and low-saline zone in pre-monsoon when the influence of freshwater inputs from rainfall and river discharge is high. Such high amplitude of intra-annual salinity variation is, however, not reported from other Indian mangroves across the Bay of Bengal coast where even larger freshwater influxes were observed (Chauhan et al. 2008). For example, the monthly average ST at Sunderban mangrove varies between 15 and 22 ppt (Das et al. 2017) that receives 1500–1800 mm rainfall annually (Rodda et al. 2016) as compared to 1267 mm at PVM. The Muthupet mangrove remains moderately saline throughout the year with the annual ST variation confined within 20–25 ppt (Krithika et al. 2008) where the annual cumulative precipitation is 1100 mm (Zade et al. 2005). Our observation clearly shows the downstream freshwater input by the rivers plays a crucial role in determining the salinity of the mangrove basin and often a strong river flow supersedes the effect of local precipitation while doing so.

The water contents in soil at various depths in the KNP ecosystem (Fig. 4b) is largely governed by the local rainfall pattern (Fig. 2d) although a delay in the occurrences of the absolute magnitudes of P_n, SM and RM are seen. Climatologically in a year the SM and RM record higher and lower values during the wetter and drier periods, respectively, at KNP. Following the annual maximum P_n of 300 mm in July (Fig. 1d) the SM and RM record maximum values of 0.37 and 0.35 $m^3 \ m^{-3}$, respectively, in August (Fig. 4). Subsequently, the SM and RM continue to decrease since September to plummet to their respective annual minimum values of 0.19 and 0.18 $m^3 \ m^{-3}$ in April (Fig. 4). Climatologically, April receives a P_n of 165 mm (Fig. 1d) replenishing the SM and RM to 0.23 and 0.20 $m^3 \ m^{-3}$ in May (Fig. 4).

Fig. 3 Mean monthly salinity (ST) and precipitation (P_n) during the analysis period at Pichavaram mangroves (PVM)
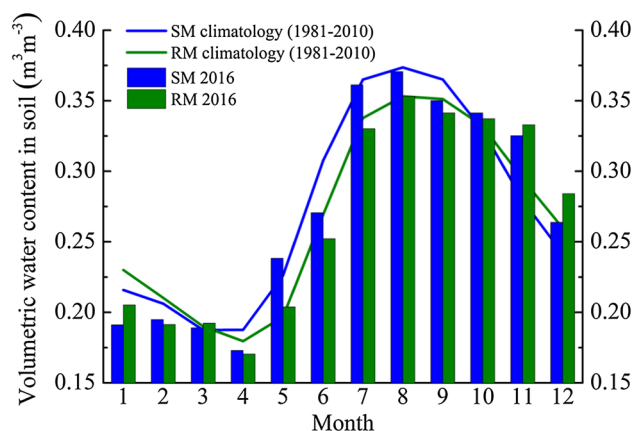

Fig. 4 Monthly mean soil moisture contents, i.e. surface soil moisture (SM) and root-zone soil moisture (RM) in 2016 and their climatological (30 years during 1981–2010) means at Kaziranga National Park (KNP) broadleaf deciduous forest

Climatologically, P_n has an increasing trend from April to July which is reflected as growing trends in SM and RM during this time. The variations of SM and RM in 2016 closely follow their climatological patterns at KNP although their absolute magnitudes vary (Fig. 4).

It is to be noticed that the SM responds faster to P_n than the RM which represents the moisture content in the deeper soil layers. During the period of increasing rainfall from April to July the SM always remains higher than RM. This can be explained as the water content in topsoil is replenished first by the rainwater which subsequently percolates to the deeper soil. As this process is slow the RM always increases at a lower rate and remains lower than SM in this period. Climatologically, from April to August the SM increases from 0.19 to 0.37 m^3 m^{-3} as compared to the RM increasing from 0.18 to 0.35 m^3 m^{-3} in the same period (Fig. 4). On a similar note, the SM also responds to the drier conditions faster than the RM. This is evident from their values during October to March when SM registers consistent lower values than RM (Fig. 4). The loss of moisture from topsoil to atmosphere is driven by the evapotranspiration process in this period as we are going to discuss later in this paper.

The monthly averaged R_g and VPD at KNP and PVM are plotted in Fig. 5. Located closer to the tropics, PVM receives higher R_g consistently throughout the year (Fig. 5a). During February to May, the PVM ecosystem receives $R_g > 500$ W m^{-2}, which explains the rising T_{air} trend during this period at this location (Fig. 2a), and together with low P_n (Fig. 2b) drives the VPD from 1.4 to 2.1 kPa in these months (Fig. 5b). In comparison, at KNP during the same period, R_g remains ≥ 350 W m^{-2} that results in the rising trend of T_{air} (Fig. 2c); P_n also increases gradually (Fig. 2d) but ground moisture remains low due to the preceding dry winter season (Fig. 4). As a result, VPD remains marginally higher than PVM at KNP. During the remaining period of the year, VPD remains much higher than KNP at PVM (Fig. 5b).

During June to September, R_g (Fig. 5a) and T_{air} (Fig. 2a) remain high and P_n (Fig. 2b) remains low which maintain the high VPD at PVM (Fig. 5b). The KNP ecosystem receives maximum P_n (Fig. 2d) in this period which replenishes the ground moisture (Fig. 4) that remains high till December, and as a result VPD remains smaller throughout this period (Fig. 5b). In sum, although located at the intersection of land and water, the PVM ecosystem experiences much higher atmospheric moisture demand. To further check this we now compare the AET and PET patterns among these two ecosystems.
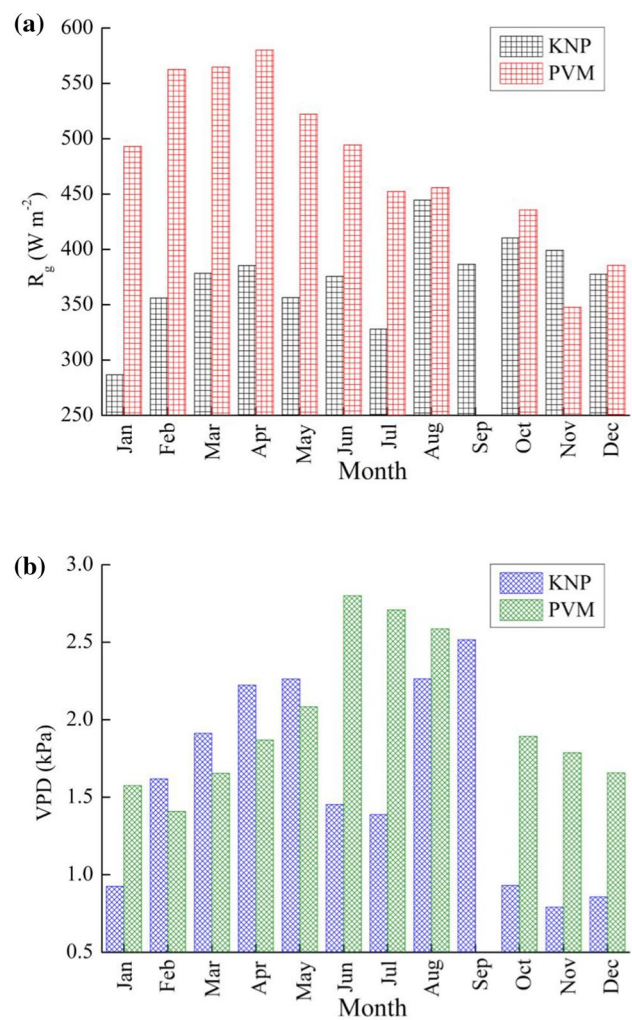

Fig. 5 Monthly averaged **a** incoming shortwave radiation (R_g) and **b** vapor pressure deficit (VPD) at Pichavaram Mangroves (PVM) and Kaziranga National Park (KNP) during the corresponding analysis periods

3.2 Actual and potential evapotranspiration

At monthly averaged scale, LE is dwarfed by PET at both the sites which is a typical of the tropical and subtropical regions (Frank and Inouye 1994). LE is always higher at KNP than PVM (Fig. 6a). However, except August PET is higher at PVM than KNP, reiterating the much larger atmospheric moisture demand at the former site. The annual maximum PET at PVM is recorded in April which is the month with maximum R_g (Fig. 5a), T_{air} (Fig. 2a) and ST (Fig. 3). In a similar fashion, the maximum PET at KNP occurs is August, driven by the annually highest R_g (Fig. 5a), T_{air} (Fig. 2c) and large VPD (Fig. 5b) in this month.
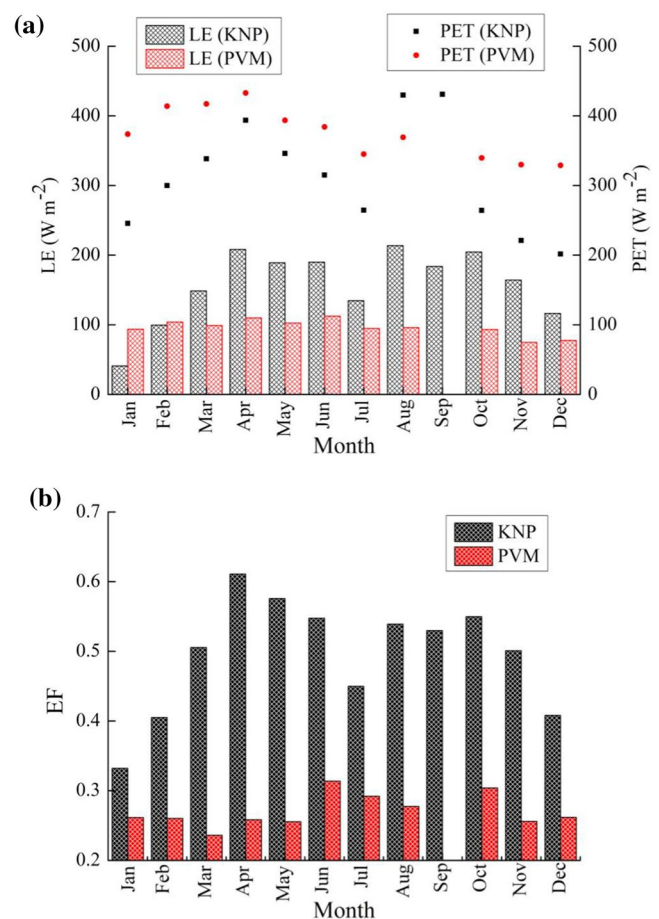
EF is much higher at KNP than PVM (Fig. 6b), including the dry winter season. Maximum EF is 0.6 at KNP, recorded in April, which is twice the value of maximum EF at PVM (Fig. 6b). EF is higher during October to December at PVM (Fig. 6b), when this ecosystem receives high rainfall (Fig. 2b) and ST remains low (Fig. 3). Moreover EF is annually lowest at PVM during February to May when ST is high (Fig. 3), despite having high R_g (Fig. 5a), T_{air} (Fig. 2a) and VPD (Fig. 5b) in these months. For a closer investigation we next investigate the different heating feedbacks by these ecosystems to the atmosphere.

3.3 Comparing the evapotranspiration between mangrove and deciduous forest

As the calendar months belong to different seasons at KNP and PVM based on the local climatology, we compare the H and LE patterns quarterly instead of seasons. The quarterly averaged half-hourly diurnal variations of H and LE (H_{av} and LE_{av}, respectively) are shown in Fig. 7. These quarters are referred in this paper as first quarter (January–March), second quarter (April to June), third quarter (July to September) and fourth quarter (October–December). The maximum values of H_{av} and LE_{av} (H_{max} and LE_{max}, respectively)

are observed around 1200 IST with prominent variations during the daytime and almost no exchange at nighttime at both sites. The values of H_{max} at PVM are 250, 260, 150 and 140 W m^{-2} in first, second, third and fourth quarters, respectively (Fig. 7a). Correspondingly the values of LE_{max} are 160, 180, 160 and 130 W m^{-2} (Fig. 7b). Hence, more available energy is partitioned towards H compared to LE in all the quarters except the third one, which is locally known as the pre-monsoon season at PVM (Kathiresan, 2000).

On the other hand, at KNP, H_{max} values are 140, 100, 90 and 120 W m^{-2}, respectively, in first, second, third and fourth quarters (Fig. 7c). At this site LE_{max} are 165, 320, 290 and 260 W m^{-2} correspondingly in these quarters (Fig. 7d). Hence, more available energy is partitioned into LE compared to H in throughout the year at KNP.

It is clearly shown that the broadleaf deciduous forest at KNP provides a larger latent heat than sensible heat transport to the atmosphere throughout the year, even during the driest season. In contrast to this, the PVM mangroves are seen to provide stronger sensible heat to the atmosphere during most of the year, which is a typical characteristic of semi-arid ecosystems (Schüttemeyer et al. 2006). Only between July and September (Fig. 7) the mangrove shows similar transport of latent and sensible heat. Here, we want
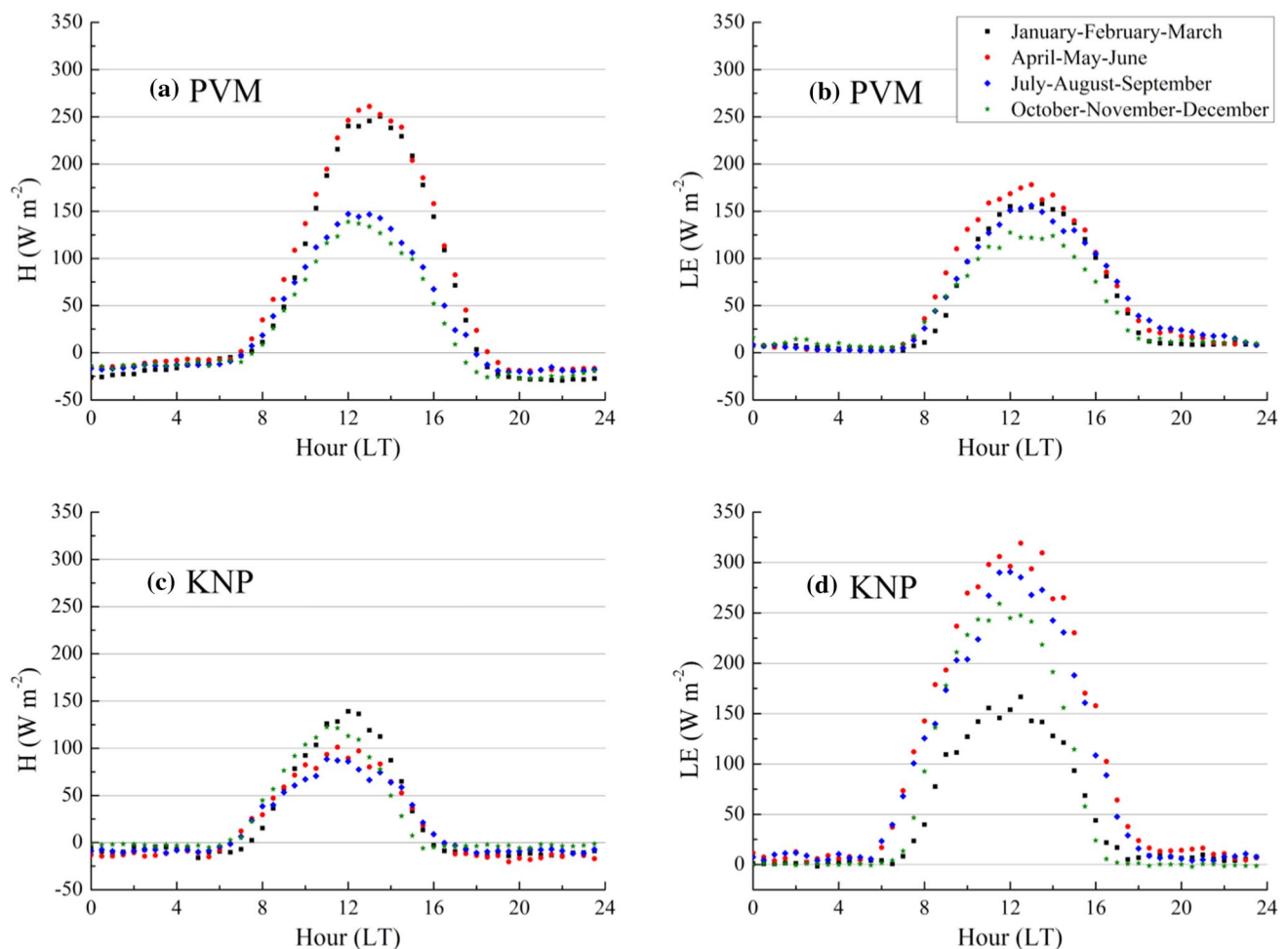
Fig. 7 Quarterly average diurnal variations of sensible (H_{av}) and latent heat fluxes (LE_{av}) computed over the monthly clusters including January to March (first quarter), April–June (second quarter), July–September (third quarter) and October–December (fourth quarter) presented as **a** H_{av} and **b** LE_{av} at the Pichavaram Mangroves (PVM) and **c** H_{av} and **d** LE_{av} at the Kaziranga National Park (KNP) during the analysis period

to highlight that the variability in H is much larger than that of LE. Thus the similar transport of H and LE is driven by a reduced H at PVM.

3.4 Relative strengths of transpiration and evaporation

We now study the relative contributions of T and E in ET at the PVM mangrove, in comparison with the broadleaf deciduous forest at KNP. The quarterly averaged half-hourly values of T and E (T_{av} and E_{av}, respectively) for both these sites are plotted in Fig. 8. Overall both the daily maximum values of T_{av} (T_{max}) and E_{av} (E_{max}) are higher at KNP than their counterparts at PVM (Fig. 8a–d). At PVM, T_{av} (Fig. 8a) is higher than E_{av} (Fig. 8b) throughout the year. T_{max} vary from 70 W m^{-2} in fourth quarter to 100 W m^{-2} in first quarter (Fig. 8a), whereas the daily maximum values of E_{av} (E_{max}) vary from 35 W m^{-2} in third quarter to 50 W m^{-2} in fourth

quarter (Fig. 8b) at PVM. Hence annually first quarter is most favorable to the transpirative activity which is defined as the post-monsoon season locally (Kathiresan 2000).

The transpirative water loss by plants is coupled with their photosynthetic uptake of carbon dioxide by stomatal opening and closure and hence this observation is also supported by the CO_2 exchange pattern of the PVM ecosystem with the atmosphere. The net ecosystem exchange (NEE in μmol m^{-2} s^{-1}) of CO_2 is the measure of the net carbon uptake by any ecosystem which is the result of its photosynthetic carbon gain (gross primary productivity or GPP) and respiratory carbon loss (ecosystem respiration or R_{eco}). The NEE of the PVM ecosystem in different seasons is plotted in Fig. 6 of (Gnanamoorthy et al. 2020) which shows the daily maximum NEE is annually largest at − 10 μmol m^{-2} s^{-1} in post-monsoon [Fig. 6b, (Gnanamoorthy et al. 2020)] and smallest at − 6 μmol m^{-2} s^{-1} in monsoon at PVM [Fig. 6a, (Gnanamoorthy et al. 2020). Table 1 of (Gnanamoorthy
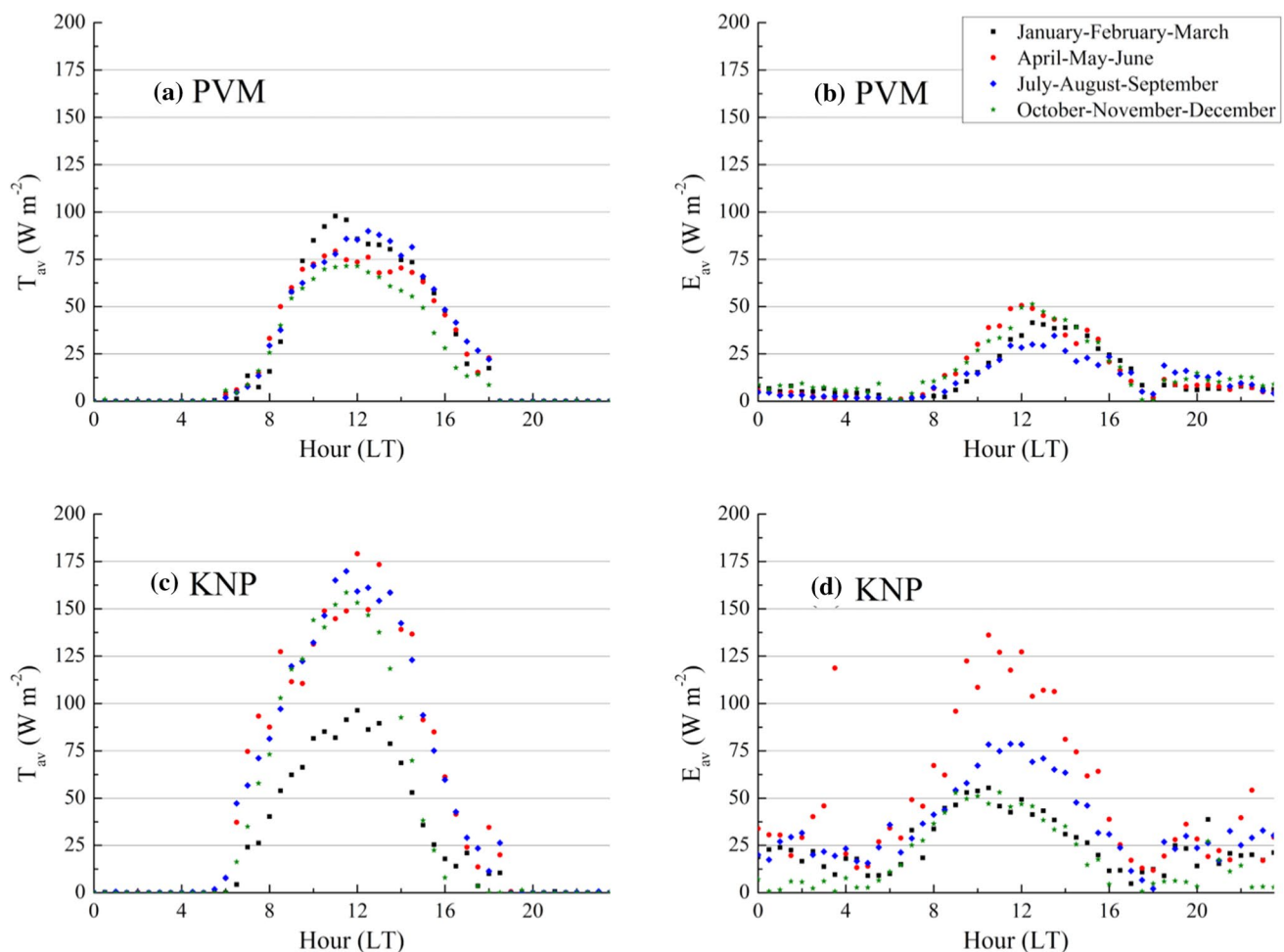
Fig. 8 Diurnal variations of averaged **a** transpiration (T_{av}) and **b** evaporation at Pichavaram Mangroves (PVM), and **c** T_{av} and **d** E_{av} at Kaziranga National Park (KNP), computed over the group of months

as indicated in the figure legend, during the corresponding analysis periods at each site

et al. 2020) lists the seasonally averaged GPP for the PVM ecosystem which is annually maximum at 4.80 gC m^{-2} day^{-1} in post-monsoon, showing the photosynthesis to be strongest in this season, also in support of our observation.

On the other hand, at KNP the T_{max} has a minimum of 100 W m^{-2} in the first quarter, (Fig. 8c) rendering this period to be least favorable for stomatal activities at KNP. This is reflected in the seasonally averaged diurnal variations of NEE at this ecosystem [Fig. 5 of (Deb Burman et al. 2020a)] as well, which is annually minimum at -5 μmol m^{-2} s^{-1} in this season. The T_{max} remains high within 150–190 W m^{-2} during second to fourth quarters (Fig. 8c). As shown in Fig. 5 of (Deb Burman et al. 2020a), the maximum NEE are also high around -13 to -15 μmol m^{-2} s^{-1} in these seasons supporting stronger stomatal activities. At KNP, T_{max} is larger than E_{max} throughout the year (Fig. 8c, d). At both KNP and PVM, T_{av} is nil at nighttime as the process of transpiration stops in the absence of incoming solar radiation.

We now study the ratio of T and ET (T/ET) during the analysis periods at KNP and PVM. Monthly box plots of T/ET for these sites are created using the 'seaborn' library (Waskom, 2021) in Python 3 in Google Colaboratory (https://colab.research.google.com/?utm_source= scs-index#scrollTo=GJBs_flRovLc), and plotted together in Fig. 9. Only the daytime values have been considered for the analysis as the nighttime exchanges are negligible [Fig. 8 of this paper and Fig. 8 of Deb Burman et al. (2019)]. Prominent seasonality in T/ET is seen at KNP. The median T/ET is larger than 0.5 during December, January and February, which constitute the winter season locally (Fig. 9). This is the annually coldest and driest season at KNP (Fig. 2c, d). The relation between T and ET mimics that of RM and SM. The increased T in this period is driven by the RM which remains higher than the SM in this season (Fig. 4b) at KNP. This is supportive of the results of Lai and Katul (2000) who show the transpirative

Fig. 9 Monthly box plots of the ratio between transpiration and evapotranspiration (T/ET) at Pichavaram Mangroves (PVM) and Kaziranga National Park (KNP), denoted as T/ET_PVM and T/ET_KNP, respectively, during the corresponding analysis periods at each site
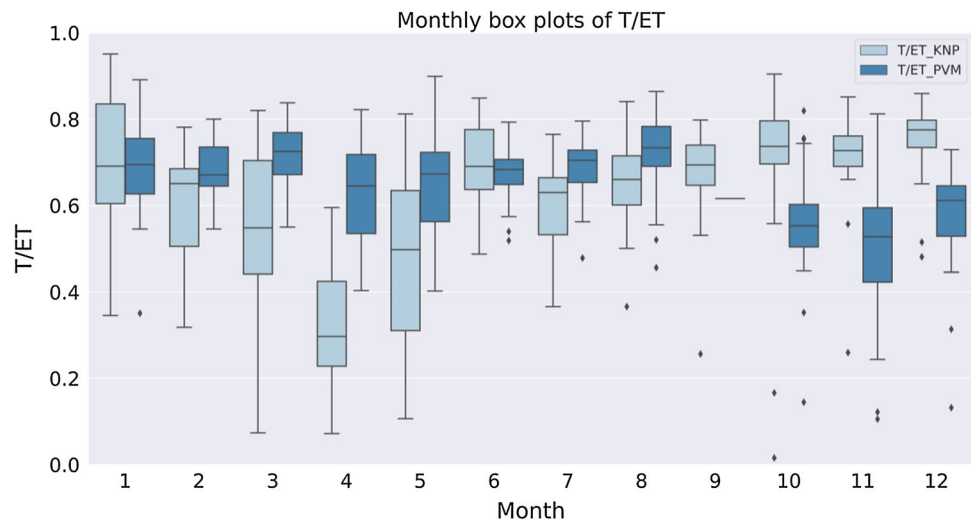

activities by plants are mostly driven by the soil water at deeper layers available to the roots for uptake while remaining largely insensitive to the surface water content variation. As E is primarily driven by SM, as pointed out by Chanzy and Bruckler (1993) it remains lower than T in this season. During March, April and May (the local pre-monsoon season) the T_{air} at KNP records an increasing trend (Fig. 2c). The KNP ecosystem also receives significant precipitation in this season (Fig. 2d) that recharges the SM (Fig. 4b). This increased SM results in enhanced E. Although the rainwater is mostly absorbed by the topsoil the RM is still comparable to SM in this season (Fig. 4b). E is seen to increase more than T in this warmer and wetter environment which reduces T/ET to ~0.5 in March, lesser than 0.6 in April and equal to 0.5 in May (Fig. 9).

In June and July, during the first half of monsoon T_{air} and P_n increases (Fig. 2c, d). Median T/ET remains larger than 0.7 in June but falls in July to increase again in August (Fig. 9). Such a dip in T/ET can be attributed to the drop in R_g in July due to the presence of dark monsoonal convective clouds as explained in Deb Burman et al. (2020a). Such a radiation-deprivation prevents the photosynthetic carbon uptake by the KNP forest ecosystem. As the carbon gain and water loss by the plants are coupled by the stomatal opening and closure mechanism the hindrance in photosynthesis is also reflected in reduced transpiration by the canopy.

The availability of radiation improves in August and September with the gradual receding of clouds from the Indian landmass increasing the photosynthetic activity (Deb Burman et al. 2020a). Subsequently, T also increases that is reflected in median T/ET values being ~0.65 (Fig. 9). Overall in monsoon season both SM and RM tables are elevated (Fig. 3b) due the increased amount of rainfall (Fig. 2d). However, the enhanced photosynthetic activity results in T larger than E in this season (Fig. 9).

During October and November, the local post-monsoon season, median T/ET remains ~0.7 (Fig. 9). P_n gradually reduces in these months (Fig. 2d). Additionally, the continued E depletes the topsoil of moisture. However, the large amount of rainwater infiltrates to the deeper soil layers by now. As a result of these the SM is lower than the RM in this season (Fig. 4). This enhanced RM drives the T which remains larger than E in post-monsoon (Fig. 9).

At PVM, T/ET is larger than unity for most of the months as found from its median values (Fig. 9). Annually, the least T/ET values are mostly observed in October, November and December when its median remains close to 0.6 (Fig. 9). These months belong to the northeast monsoon season characterized by the annually coldest environment with the highest P_n (Fig. 2b) and lowest R_g (Fig. 4a). Also the water in the mangrove wetland is less saline (ST < 20 ppt) during this
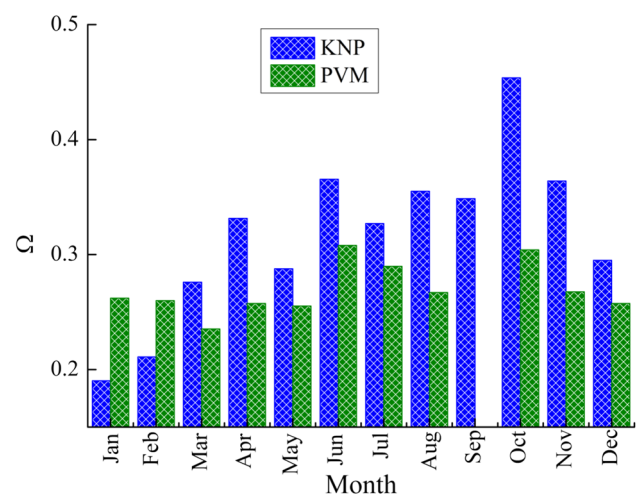
Fig. 10 Monthly averaged canopy–atmosphere decoupling coefficient (Ω) at Pichavaram Mangroves (PVM) and Kaziranga National Park (KNP) during the corresponding analysis periods

period (Fig. 3a). Hence T is seen to be the dominant component of ET throughout the year. While ET in dry seasons is mostly driven by T, the contribution of E increases during the wet period. This shows the E to be more sensitive to the environmental conditions compared to T at PVM. Overall, we find T/ET to be fluctuating more at KNP compared to PVM. The ratio of T and E (T/E) is another analogous interpretation of the relative strengths of T and E. The monthly box plots of T/E at both the sites are provided in supplementary figure S2.

To further explore the biosphere–atmosphere interaction, next we study the variability of Ω at these two ecosystems. At monthly averaged scale daytime Ω remains confined to 0.3 throughout the year at PVM (Fig. 10). Such smaller values of Ω signify tighter physiological control on canopy water exchange with atmosphere. This reiterates our earlier finding that ET by this mangrove ecosystem is primarily controlled by T (Fig. 9a). Interestingly, Ω is lower during February–May (Fig. 10) which also corresponds to the higher ST (Fig. 3) and lower P_n at this site (Fig. 2b). On the other hand, annually higher Ω is observed during October to December when ST is low (Fig. 3) and P_n is high (Fig. 2b).

To summarize, during the period with highest ST at PVM (March–April–May) high stomatal control is observed. On the other hand, during the lowest ST period (July–August) highest VPD is recorded, simultaneously with larger values of Ω indicating a reduced stomatal control. Specifically in June, ST still remains high but the large VPD in this month dictates the stomatal control over the salinity. Hence at low VPD, ST has negative impact on T but the control of VPD grows stronger with its value. Since the water loss from the ecosystem to the atmosphere increases with VPD, it increases the water salinity and hence, results in a negative correlation between VPD and ST. In fact Ω is high implying lesser stomatal control during the period with low-medium salinity and low-medium VPD (October–November–December) at PVM, which supports our hypothesis.

At KNP Ω is higher than PVM during March to December implying the environmental control on water exchange to be stronger at the broadleaf deciduous forest compared to the mangrove (Fig. 10). In January and February Ω at KNP is less than PVM when physiological controls are larger at KNP than PVM (Fig. 10). Overall Ω is lower in the dry months and higher in wet months at KNP (Fig. 10) as also found by Kumagai et al. (2004) and Bracho et al. (2008) at several other tropical forest ecosystems.

G_s is much lower at PVM (Fig. 11a) than KNP (Fig. 11b) highlighting more favorable conditions for atmospheric water vapor exchange at the broadleaf deciduous forest throughout the year compared to its mangrove counterpart as evident from their monthly median values. Interestingly at PVM, annually lowest values occurrences of G_s coincide
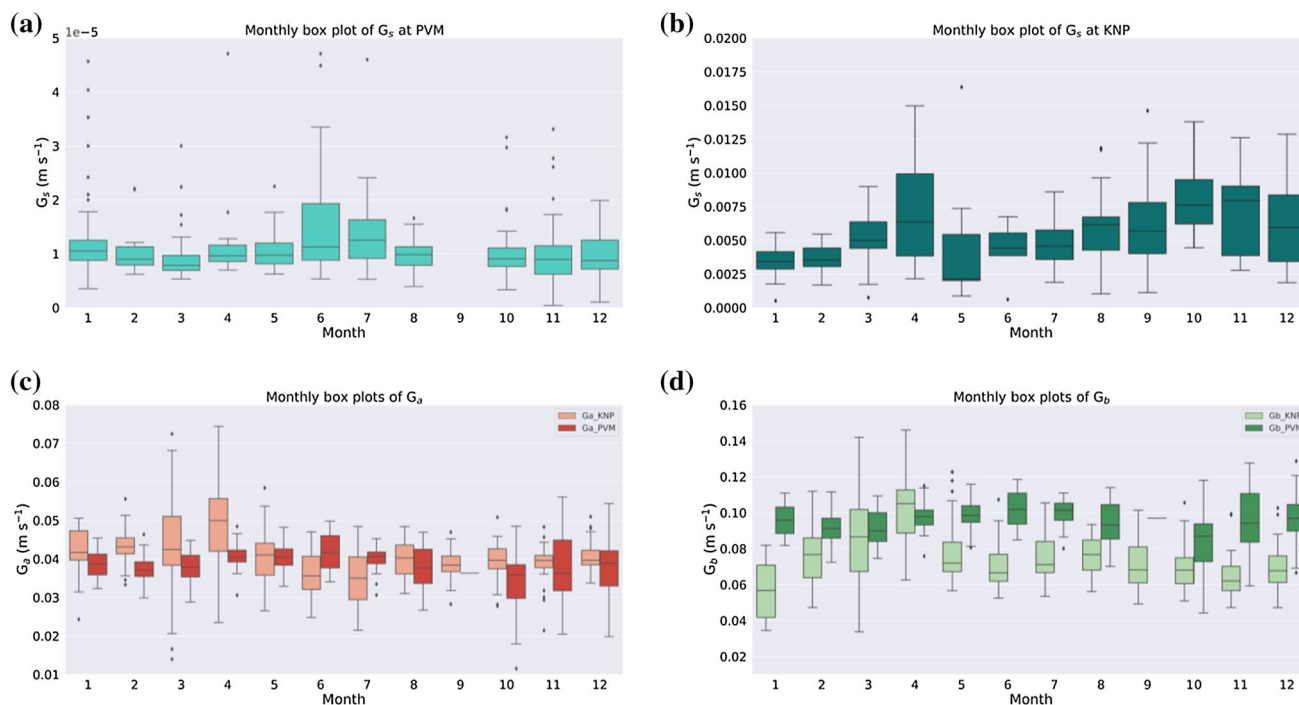
Fig. 11 Monthly box plots of **a** surface conductance to water vapor (G_s) at Pichavaram Mangroves (PVM), **b** G_s at Kaziranga National Park (KNP), **c** aerodynamic conductances (G_a) at KNP and PVM (denoted as Ga_KNP and Ga_PVM, respectively) and **d** boundary layer conductances (G_b) at PVM and KNP (denoted as Gb_KNP and Gb_PVM, respectively) during the corresponding analysis periods at each site. Note that the scales on y-axes are differing among the panels

with the high ST periods (Fig. 3) and vice versa (Fig. 11a) clearly indicating the role of salinity in determining this variable. On the other hand, G_s are low and high during dry and wet periods, respectively, at KNP (Fig. 10b).

G_b remains higher than or comparable to G_a at both these sites as expected (Figs. 10c-d). However, G_b is consistently higher at PVM than its KNP analogue (Fig. 10d) throughout the year. In fact, G_b increases during February–June at PVM (Fig. 10d), which are the months with high ST (Fig. 3a). These observations clearly show that although the environmental turbulence and mixing are favorable for water vapor exchange, it is practically limited by ST through the latter's

physiological control. We now assess the controlling mechanisms of T and E at both these ecosystems.

3.5 Meteorological controls on transpiration and evaporation

Different meteorological parameters affect T and E in different capacities. Plants tend to transpire more water for reducing their leaf temperature in warmer environment. Evaporative loss of water is also high in such conditions. The canopy transpirative loss of water is accelerated at moderately high atmospheric demand of moisture which is reflected in VPD
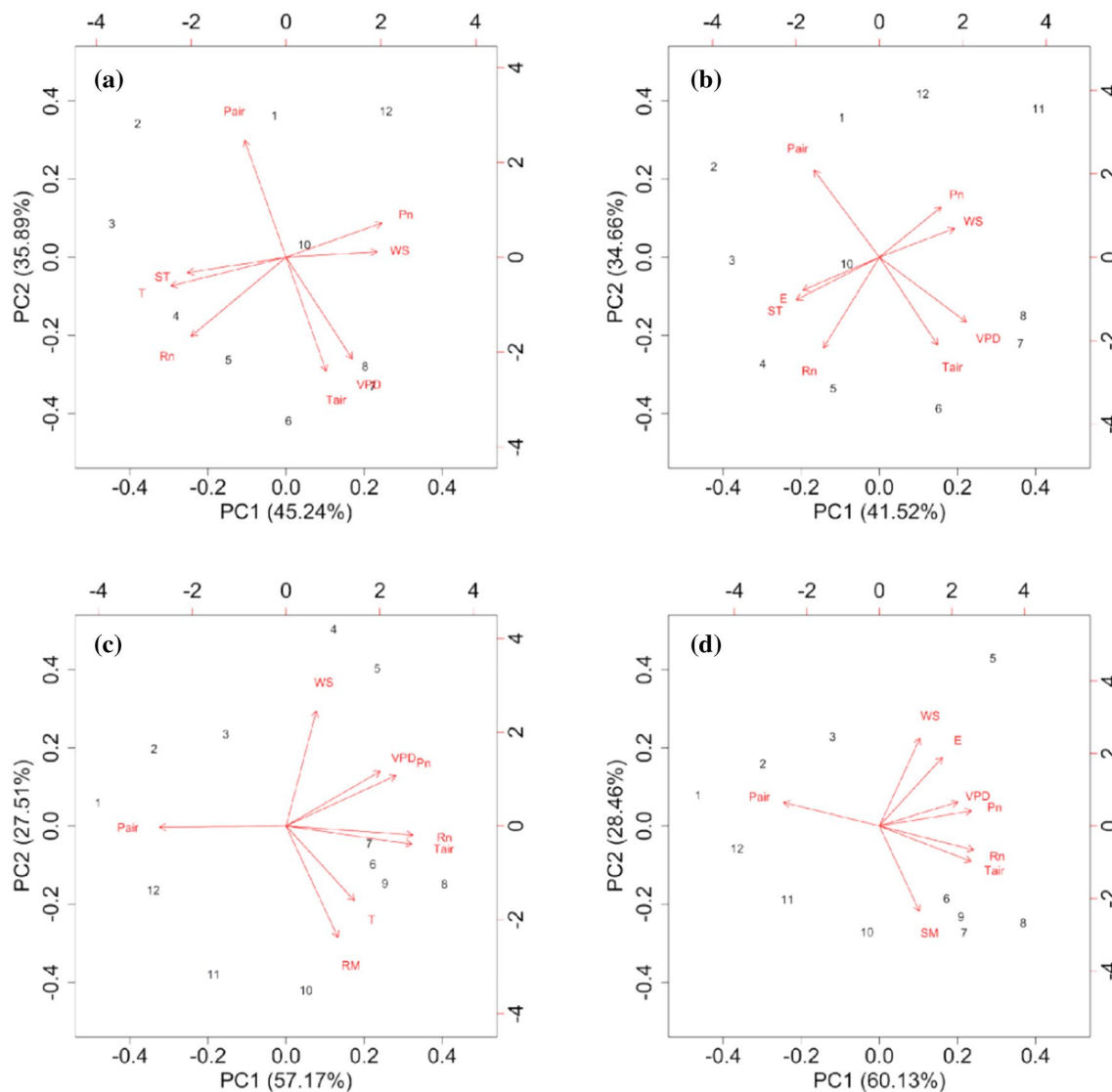
Fig. 12 Biplots of Principal Component Analyses of monthly averaged **a** transpiration (T), **b** evaporation (E) at Pichavaram Mangroves, **c** T and **d** E at Kaziranga National Park as functions of air temperature (T_{air}), air pressure (P_{air}), precipitation (P_n), surface soil moisture (SM), root-zone soil moisture (RM), vapor pressure deficit (VPD), horizontal wind speed (WS), and net radiation (R_n) during the cor-

responding analysis periods. The horizontal and vertical axes in each of the subplots show the first and second principal components (PC1 and PC2, respectively) with the corresponding percentage of variations explained by those in the parentheses. The numbers in each plot represent the corresponding measurement month (i.e. 1 stands for January, 12 stands for December, etc.)

(Jarvis and Mcnaughton 1986) before it reduces again due to stomatal closure at high values of VPD. The VPD is also responsible for increasing E by accelerating the evaporative demand. Radiation is the primary source of energy that is allocated in different components of surface energy budget including E and T. Surface wind affects T and E by changing the surface atmospheric conditions and mixing (Jarvis and Mcnaughton 1986). Negative feedbacks are seen in the relation of ST with T and E. While increased ST arrests T and E, increment in either of these in turn increases ST (Passioura et al. 1992). We use PCA in this section to find the most dominant controls on T and E and compare the outcomes between a mangrove and a broadleaf deciduous forest.

Figure 12a shows the PCA biplot for T at PVM. The first two PCs account for 81.13% of the variations in T (Table 1) justifying the two-dimensional representation of the variables in Fig. 12a. The strongest correlation of T is observed with ST. The second strongest correlation of T is seen with R_n. Negative correlations of T are observed with P_n and WS. There is almost a lack of correlation of T with P_{air}, T_{air} and VPD. The PCA biplot for E at PVM is shown is Fig. 12b. The first two PCs account for 76.19% of the variations (Table 1). The strongest correlation of E is seen with ST with the next largest correlation with R_n. Negative correlations of E are seen with P_n and WS whereas almost no correlation of E exists with T_{air}, P_{air} and VPD.

At KNP the PCA biplot for T is shown in Fig. 12c. The first two PCs account for 84.68% of the variations (Table 1). The largest correlation of T is seen with RM with the second largest correlation with T_{air}. Subsequently, larger correlation of T is observed with R_n comparable to T_{air}. Small but positive correlations of T are observed with P_n and VPD while P_{air} and WS have negative correlations with T. Finally, the PCA biplot for E at KNP is shown in Fig. 12d. The first two PCs explain 88.59% variations (Table 1) in the data. The strongest correlation of E is observed with WS and the next largest correlation with VPD. Additionally, E has positive correlations with P_n, R_n and T_{air} and negative correlation with SM and P_{air}. In contrast with PVM, T_{air} has stronger correlation with T at KNP. Also E at PVM does not have strong dependencies on WS and VPD as compared to KNP.

3.6 Comparison with other mangrove ecosystems

The evapotranspiration from Pichavaram mangrove is reported for the first time in the present study. Estimating ET and its drivers in mangroves remains a challenge due to the submerged nature of the soil (Drexler et al. 2004) and very few studies so far have reported these using in situ measurements (Baldocchi, 2003). In contrast to PVM, LE remains higher than H throughout the year at Sundarban mangrove (Ganguly et al. 2008; Chanda et al. 2013), however, the independent estimates of T and E at this ecosystem are not available till writing this paper. At the Phangnga Bay

National Park mangrove in southern Thailand T is higher in dry season than wet season (Hirano et al. 1996) similar to PVM, although in this ecosystem R_n and humidity are the primary drivers of T as compared to ST and R_n at PVM. According to Krauss et al. (2015) stand water use, a close measure of T constitutes 34–66% of ET at three mangrove sites in southwest Florida, USA.

4 Conclusions

The different diverse ecosystems in India spread over a large geoclimatic span, play crucial roles in the hydrological and energy cycles and provide important heating response to the atmosphere driving the conduction and mixing processes. Proper representation of these transport processes, their seasonality and drivers are not only necessary to improve the performance of numerical weather prediction and hydrological models but also important to represent these ecosystem types in ecosystem, Earth system and climate models, however, presently remain poorly explored due to the paucity of surface measurements over this region. In this context, we have studied the evapotranspiration, its components and drivers at a tropical mangrove at Pichavaram and comparatively assessed the same against a broadleaf deciduous forest ecosystem at the Kariranga National Park in India using in situ eddy covariance measurements in the present work. Following are the key outcomes this study:

1. The tropical mangrove at Pichavaram is seen to provide maximum heating to the atmosphere as 'dry' sensible heat during most of the year similar to a semi-arid ecosystem. During the pre-monsoon season it switches this behavior akin to a well-watered ecosystem when the evapotranspirative 'moist' heat feedback becomes dominating.

2. This is in contrast with the broadleaf deciduous forest at the Kaziranga National Park which provides stronger evapotranspirative feedback throughout the year and hence performs as a well-watered ecosystem even in the dry season.

3. The ecosystem–atmosphere coupling is stronger at the mangrove than the broadleaf deciduous forest.

4. Transpiration is the major component of evapotranspiration by Pichavaram mangrove throughout most of the year, in contrast with the broadleaf deciduous forest where transpiration and evaporation dominate each other during the different periods of year.

5. The transpiration by the mangrove is most strongly coupled with salinity as compared to air temperature for the broadleaf deciduous forest, followed by radiation in both the ecosystems.

6. Salinity is also most tightly coupled with the evaporation from the mangrove, followed by radiation. On the other hand, evaporation from the broadleaf deciduous forest is most strongly coupled with wind speed and radiation.

As compared to other natural ecosystems, studies reporting ET and their dependencies on environmental variables in mangroves are rather less due to the complexity in measuring and modelling the same because of the submerged nature of these ecosystems (Drexler et al. 2004). Salinity regulation of transpiration has an important implication for the carbon cycle of these ecosystems as decreased transpiration ensues reduced photosynthesis hindering the growth of mangrove biomass eventually resulting in forest dieback (Cintron et al. 1978; Sippo et al. 2018). Our study will be useful to the modelling community in these regards for better parameterizing the ecophysiological processes in models.

Code availability Not applicable.

Declarations

Conflicts of interest/Competing interest The authors declare no competing interest.

References

Aitchison J, Greenacre M (2002) Biplots of compositional data. J R Stat Soc Ser C Appl Stat 51:375–392. https://doi.org/10.1111/1467-9876.00275

Akhand A, Chanda A, Manna S, Das S, Hazra S, Roy R, Choudhury SB, Rao KH, Dadhwal VK, Chakraborty K, Mostofa KMG, Tokoro T, Kuwae T, Wanninkhof R (2016) A comparison of CO2 dynamics and air-water fluxes in a river-dominated estuary and a mangrove-dominated marine estuary. Geophys Res Lett 43:11726–11735. https://doi.org/10.1002/2016GL070716

Allen RG, Pereira LS, Raes D, Smith M (1998) Crop evapotranspiration: Guidelines for computing crop requirements, Irrigation and Drainage Paper No. 56, FAO. Rome.

Alongi DM (2014) Carbon Cycling and Storage in Mangrove Forests. Ann Rev Mar Sci 6:195–219. https://doi.org/10.1146/annurev-marine-010213-135020

Aubinet M, Vesala T, Papale D (2012) Eddy covariance: apractical guide to measurement and data analysis. Springer Science & Business Media.https://doi.org/10.1007/978-94-007-2351-1

Aussenac G (2000) Interactions between forest stands and microclimate: Ecophysiological aspects and consequences for silviculture. Ann for Sci. https://doi.org/10.1051/forest:2000119

Baldocchi DD (2003) Assessing the eddy covariance technique for evaluating carbon dioxide exchange rates of ecosystems: Past, present and future. Glob Change Biol 9:479–492. https://doi.org/10.1046/j.1365-2486.2003.00629.x

Barr JG, Delonge MS, Fuentes JD (2014) Seasonal evapotranspiration patterns in mangrove forests. J Geophys Res 119:3886–3899. https://doi.org/10.1002/2013JD021083

Barros VR, Field CB, Dokken DJ, Mastrandrea MD, Mach KJ, Bilir TE, Chatterjee M, Ebi KL, Estrada YO, Genova RC, Girma B, Kissel ES, Levy AN, MacCracken S, Mastrandrea PR, White LL (2014) Climate change 2014 impacts, adaptation, and vulnerability Part B: Regional aspects: Working group ii contribution to the fifth assessment report of the intergovernmental panel on climate change, Climate Change 2014: Impacts, Adaptation and Vulnerability: Part B: Regional Aspects: Working Group II Contribution to the Fifth Assessment Report of the Intergovernmental Panel on Climate Change. https://doi.org/10.1017/CBO9781107415386

Beck HE, Zimmermann NE, McVicar TR, Vergopolan N, Berg A, Wood EF (2018) Present and future köppen-geiger climate classification maps at 1-km resolution. Sci Data. https://doi.org/10.1038/sdata.2018.214

Berger U, Rivera-Monroy VH, Doyle TW, Dahdouh-Guebas F, Duke NC, Fontalvo-Herazo ML, Hildenbrandt H, Koedam N, Mehlig U, Piou C, Twilley RR (2008) Advances and limitations of individual-based models to analyze and predict dynamics of mangrove forests: A review. Aquat Bot 89:260–274. https://doi.org/10.1016/j.aquabot.2007.12.015

Bonan G (2015) Ecological climatology: concepts and applications. Cambridge University Press. https://doi.org/10.21425/f58433332

Bongaarts J (2019) IPBES, 2019. Summary for policymakers of the global assessment report on biodiversity and ecosystem services of the Intergovernmental Science-Policy Platform on Biodiversity and Ecosystem Services. Popul Dev Rev. https://doi.org/10.1111/padr.12283

Boyer TP, Levitus S (2002) Harmonic analysis of climatological sea surface salinity. J Geophys Res C Ocean 107:8006. https://doi.org/10.1029/2001jc000829

Bracho R, Powell TL, Dore S, Li J, Hinkle CR, Drake BG (2008) Environmental and biological controls on water and energy exchange in Florida scrub oak and pine flatwoods ecosystems. J Geophys Res Biogeosci 113:G02004. https://doi.org/10.1029/2007JG000469

Bréda N, Huc R, Granier A, Dreyer E (2006) Temperate forest trees and stands under severe drought: a review of ecophysiological responses, adaptation processes and long-term consequences. Ann for Sci 63:625–644. https://doi.org/10.1051/forest:2006042

Campbell GS, Norman JM (2000) An introduction to environmental biophysics. Springer Science & Business Media. https://doi.org/10.1007/978-1-4612-1626-1

Chakraborty S, Tiwari YK, Deb Burman PK, Baidya Roy S, Valsala V, Gupta S, Metya A, Gahlot S (2020) Observations and modeling of ghg concentrations and fluxes over India. In: Assessment of climate change over the Indian Region. Springer Nature. https://doi.org/10.1007/978-981-15-4327-2_4

Chanda A, Akhand A, Manna S, Dutta S, Hazra S, Das I, Dadhwal VK (2013) Characterizing spatial and seasonal variability of carbon dioxide and water vapour fluxes above a tropical mixed mangrove forest canopy, India. J Earth Syst Sci 122:503–513. https://doi.org/10.1007/s12040-013-0288-9

Chanzy A, Bruckler L (1993) Significance of soil surface moisture with respect to daily bare soil evaporation. Water Resour Res 29:1113–1125. https://doi.org/10.1029/92WR02747

Chauhan R, Ramanathan AL, Adhya TK (2008) Assessment of methane and nitrous oxide flux from mangroves along Eastern coast of India. Geofluids 8:321–332. https://doi.org/10.1111/j.1468-8123.2008.00227.x

Cintron G, Lugo AE, Pool DJ, Morris G (1978) Mangroves of arid environments in Puerto Rico and adjacent islands. Biotropica 2:110–121. https://doi.org/10.2307/2388013

Crow WT (2007) A novel method for quantifying value in spaceborne soil moisture retrievals. J Hydrometeorol 8:56–67. https://doi.org/10.1175/JHM553.1

Dai Y, Dickinson R, Wang Y (2004) A two-big-leaf model for canopy temperature, photosynthesis, and stomatal conductance. J Clim 17:2281–2299. https://doi.org/10.1175/1520-0442(2004)017%3c2281:ATMFCT%3e2.0.CO;2

Das S, Ganguly D, Ray R, Jana TK, De TK (2017) Microbial activity determining soil CO2 emission in the Sundarban mangrove forest. India Trop Ecol 58:535–537

Datta D, Deb S (2012) Analysis of coastal land use/land cover changes in the Indian Sunderbans using remotely sensed data. Geo-Spatial Inf Sci 15:241–250. https://doi.org/10.1080/10095020.2012.714104

Deb Burman PK, Sarma D, Williams M, Karipot A, Chakraborty S (2017) Estimating gross primary productivity of a tropical forest ecosystem over north-east India using LAI and meteorological variables. J Earth Syst Sci 126:1–16. https://doi.org/10.1007/s12040-017-0874-3

Deb Burman PK, Sarma D, Morrison R, Karipot A, Chakraborty S (2019) Seasonal variation of evapotranspiration and its effect on the surface energy budget closure at a tropical forest over north-east India. J Earth Syst Sci 128:1–21. https://doi.org/10.1007/s12040-019-1158-x

Deb Burman PK, Sarma D, Chakraborty S, Karipot A, Jain AK (2020a) The effect of Indian summer monsoon on the seasonal variation of carbon sequestration by a forest ecosystem over North-East India. SN Appl Sci 2:154. https://doi.org/10.1007/s42452-019-1934-x

Deb Burman PK, Shurpali NJ, Chowdhuri S, Karipot A, Chakraborty S, Lind SE, Martikainen PJ, Chellappan S, Arola A, Tiwari YK, Murugavel P, Gurnule D, Todekar K, Prabha TV (2020b) Eddy covariance measurements of CO2 exchange from agro-ecosystems located in subtropical (India) and boreal (Finland) climatic conditions. J Earth Syst Sci 129(1). https://doi.org/10.1007/s12040-019-1305-4

Deb Burman PK, Launiainen S, Mukherjee S, Chakraborty S, Gogoi N, Murkute C, Lohani P, Sarma D, Kumar K (2021) Ecosystem-atmosphere carbon and water exchanges of subtropical evergreen and deciduous forests in India. For Ecol Manag 495:119371. https://doi.org/10.1016/j.foreco.2021.119371

Donato DC, Kauffman JB, Murdiyarso D, Kurnianto S, Stidham M, Kanninen M (2011) Mangroves among the most carbon-rich forests in the tropics. Nat Geosci 4:293–297. https://doi.org/10.1038/ngeo1123

Drexler JZ, Snyder RL, Spano D, Paw UKT (2004) A review of models and micrometeorological methods used to estimate wetland evapotranspiration. Hydrol Process 18:2071–2101. https://doi.org/10.1002/hyp.1462

Fisher JB, Whittaker RJ, Malhi Y (2011) ET come home: potential evapotranspiration in geographical ecology. Glob Ecol Biogeogr 20:1–18. https://doi.org/10.1111/j.1466-8238.2010.00578.x

Frank DA, Inouye RS (1994) Temporal variation in actual evapotranspiration of terrestrial ecosystems: patterns and ecological implications. J Biogeogr 21:401–411. https://doi.org/10.2307/2845758

Gabriel KR (1971) The biplot graphic display of matrices with application to principal component analysis. Biometrika 58:453–467. https://doi.org/10.1093/biomet/58.3.453

Ganguly D, Dey M, Mandal SK, De TK, Jana TK (2008) Energy dynamics and its implication to biosphere-atmosphere exchange of CO2, H2O and CH4 in a tropical mangrove forest canopy. Atmos Environ 42:4172–4184. https://doi.org/10.1016/j.atmosenv.2008.01.022

Gentine P, Entekhabi D, Chehbouni A, Boulet G, Duchemin B (2007) Analysis of evaporative fraction diurnal behaviour. Agric for Meteorol 143:13–29. https://doi.org/10.1016/j.agrformet.2006.11.002

Giri C, Long J, Abbas S, Murali RM, Qamer FM, Pengra B, Thau D (2015) Distribution and dynamics of mangrove forests of South Asia. J Environ Manag 148:101–111. https://doi.org/10.1016/j.jenvman.2014.01.020

Gnanamoorthy P, Selvam V, Ramasubramanian R, Nagarajan R, Chakraborty S, Deb Burman PK, Karipot A (2019) Diurnal and seasonal patterns of soil CO2 efflux from the Pichavaram mangroves, India. Environ Monit Assess 191:1–12. https://doi.org/10.1007/s10661-019-7407-2

Gnanamoorthy P, Selvam V, Deb Burman PK, Chakraborty S, Karipot A, Nagarajan R, Ramasubramanian R, Song Q, Zhang Y, Grace J (2020) Seasonal variations of net ecosystem (CO2) exchange in the Indian tropical mangrove forest of Pichavaram. Estuar Coast Shelf Sci 243:106828. https://doi.org/10.1016/j.ecss.2020.106828

Gnanappazham L, Selvam V (2014) Response of mangroves to the change in tidal and fresh water flow—a case study in Pichavaram, South India. Ocean Coast Manag 102:131–138. https://doi.org/10.1016/j.ocecoaman.2014.09.004

Hand D, Mannila H, Smyth P (2001) Principles of data mining. MIT Press, Cambridge. https://doi.org/10.1007/978-1-4471-4884-5

Hicks BB, Baldocchi DD, Meyers TP, Hosker RP, Matt DR (1987) A preliminary multiple resistance routine for deriving dry deposition velocities from measured quantities. Water Air Soil Pollut 36:311–330. https://doi.org/10.1007/BF00229675

Hirano T, Monji N, Hamotani K, Jintana V, Yabuki K (1996) Transpirational characteristics of mangrove species in Southern Thailand. Environ Control Biol 34:285–293. https://doi.org/10.2525/ecb1963.34.285

Hughes CE, Kalma JD, Binning P, Willgoose GR (2001) Estimating evapotranspiration for a temperate salt marsh, Newcastle, Australia. Hydrol Process 15:957–975. https://doi.org/10.1002/hyp.189

India State of Forest Report (2019) Ministry of environment, forest & climate change. Government of India, Dehradun

IPCC (2013a) 2013 supplement to the 2006 guidelines: wetlands, thirty-seventh session of the IPCC. IPCC

IPCC (2013b) 2013 Supplement to the 2006 IPCC guidelines for national greenhouse gas inventories: wetlands. IPCC

Ivanov MA, Evtimov SN (2014) Seasonality in the biplot of Northern Hemisphere temperature anomalies. Q J R Meteorol Soc 140:2650–2657. https://doi.org/10.1002/qj.2332

Jain SK, Kumar V (2012) Trend analysis of rainfall and temperature data for India. Curr Sci 102:37–49

Jarvis PG, Mcnaughton KG (1986) Stomatal control of transpiration: scaling up from leaf to region. Adv Ecol Res 15:1–49. https://doi.org/10.1016/S0065-2504(08)60119-1

Jaswal AK, Narkhede NM, Shaji R (2014) Atmospheric data collection, processing and database management in India meteorological department. Proc Indian Natl Sci Acad 80:697–704. https://doi.org/10.16943/ptinsa/2014/v80i3/55144

Jolliffe IT (2002) Principal component analysis, second edition. In: Springer Series in Statistics. Springer-Verlag, New York, https://doi.org/10.1007/b98835

Jollife IT, Cadima J (2016) Principal component analysis: A review and recent developments. Philos Trans R Soc A Math Phys Eng Sci. https://doi.org/10.1098/rsta.2015.0202

Kathiresan K (2000) A review of studies on Pichavaram mangrove, southeast India. Hydrobiologia 430:185–205. https://doi.org/10.1023/A:1004085417093

Katul GG, Palmroth S, Oren RAM (2009) Leaf stomatal responses to vapour pressure deficit under current and CO2-enriched atmosphere explained by the economies of gas exchange. Plant Cell Environ 32:968–979

Knauer J, El-Madany TS, Zaehle S, Migliavacca M (2018) Bigleaf—an R package for the calculation of physical and physiological ecosystem properties from eddy covariance data. PLoS ONE 13:e0201114. https://doi.org/10.1371/journal.pone.0201114

Kool D, Agam N, Lazarovitch N, Heitman JL, Sauer TJ, Ben-Gal A (2014) A review of approaches for evapotranspiration partitioning. Agric for Meteorol 184:56–70. https://doi.org/10.1016/j.agrformet.2013.09.003

Krauss KW, Barr JG, Engel V, Fuentes JD, Wang H (2015) Approximations of stand water use versus evapotranspiration from three mangrove forests in southwest Florida. USA Agric for Meteorol 213:291–303. https://doi.org/10.1016/j.agrformet.2014.11.014

Kripa MK, Nivas AH, Lele N, Thangaradjou T, Kumar AS, Mankad AU, Murthy TVR (2019) Seasonal dynamics and light use efficiency of major mangrove species over Indian Region. Proc Natl Acad Sci India Sect B Biol Sci. https://doi.org/10.1007/s40011-019-01077-x

Krithika K, Purvaja R, Ramesh R (2008) Fluxes of methane and nitrous oxide from an Indian mangrove. Curr Sci 94:218–224

Kumagai T, Katul GG, Porporato A, Saitoh TM, Ohashi M, Ichie T, Suzuki M (2004) Carbon and water cycling in a Bornean tropical rainforest under current and future climate scenarios. Adv Water Resour 27:1135–1150. https://doi.org/10.1016/j.advwatres.2004.10.002

Kumar D, Scheiter S (2019) Biome diversity in South Asia—how can we improve vegetation models to understand global change impact at regional level? Sci Total Environ 671:1001–1016. https://doi.org/10.1016/j.scitotenv.2019.03.251

Lai CT, Katul G (2000) The dynamic role of root-water uptake in coupling potential to actual transpiration. Adv Water Resour 23:427–439. https://doi.org/10.1016/S0309-1708(99)00023-8

Laubach J, Kellihar FM (2004) Measuring methane emission rates of a dairy cow herd by two micrometeorological techniques. Agric for Meteorol 125:289–303. https://doi.org/10.1016/j.agrformet.2004.04.003

Luo Z, Sun OJ, Wang E, Ren H, Xu H (2010) Modeling productivity in mangrove forests as impacted by effective soil water availability and its sensitivity to climate change using biome-BGC. Ecosystems 13:949–965. https://doi.org/10.1007/s10021-010-9365-y

Maes WH, Gentine P, Verhoest NEC, Miralles DG (2019) Potential evaporation at eddy-covariance sites across the globe. Hydrol Earth Syst Sci 23:925–948. https://doi.org/10.5194/hess-23-925-2019

Mahanta R, Sarma D, Choudhury A (2013) Heavy rainfall occurrences in northeast India. Int J Climatol 33:1456–1469. https://doi.org/10.1002/joc.3526

Mair P (2018) Principal component analysis and extensions. Springer, Cham. https://doi.org/10.1007/978-3-319-93177-7_6

Mardia KV, Kent JT, Bibby JM (1997) Multivariate analysis, 1st edn. Academic Press, London

Marois DE, Mitsch WJ (2015) Coastal protection from tsunamis and cyclones provided by mangrove wetlands—a review. Int J Biodivers Sci Ecosyst Serv Manag 11:71–83. https://doi.org/10.1080/21513732.2014.997292

Martens B, Miralles DG, Lievens H, Van Der Schalie R, De Jeu RAM, Fernández-Prieto D, Beck HE, Dorigo WA, Verhoest NEC (2017) GLEAM v3: Satellite-based land evaporation and root-zone soil moisture. Geosci Model Dev 10:1903–1925. https://doi.org/10.5194/gmd-10-1903-2017

Mauder M, Foken T (2004) Documentation and Instruction Manual of the Eddy-Covariance Software Package TK3 (update). Bayreuth

McMillan AMS, Harvey MJ, Martin RJ, Bromley AM, Evans MJ, Mukherjee S, Laubach J (2014) The detectability of nitrous oxide mitigation efficacy in intensively grazed pastures using a multiple-plot micrometeorological technique. Atmos Meas Tech 7:1169–1184. https://doi.org/10.5194/amt-7-1169-2014

Metya A, Chakraborty S, Bhattacharya SK, Datye A., Deb Burman PK, Dasgupta P, et al. (2021) Isotopic and concentration analyses of CO_2 and CH_4 in association with the eddy-covariance based measurements in a tropical forest of northeast India. Earth and Space Science 8:e2020EA001504. https://doi.org/10.1029/2020EA001504

Miralles DG, De Jeu RAM, Gash JH, Holmes TRH, Dolman AJ (2011) Magnitude and variability of land evaporation and its components at the global scale. Hydrol Earth Syst Sci 15:967–981. https://doi.org/10.5194/hess-15-967-2011

Monteith JL et al (1965) Evaporation and environment. In: Symposia of the society for experimentalbiology. vol 19. Cambridge University Press (CUP), Cambridge

Morison JI, Gifford RM (1983) Stomatal sensitivity to carbon dioxide and humidity: a comparison of two C3 and two C4 grass species. Plant Physiol 71:789–796

Mukherjee S, McMillan AMS, Sturman AP, Harvey MJ, Laubach J (2015) Footprint method to separate N2O emission rates from adjacent paddock areas. Int J Biometeorol 59:325–338. https://doi.org/10.1007/s00484-014-0844-2

Nelson JA, Pérez-Priego O, Zhou S, Poyatos R, Zhang Y, Blanken PD, Gimeno TE, Wohlfahrt G, Desai AR, Gioli B, Limousin J-M, Bonal D, Paul-Limoges E, Scott RL, Varlagin A, Fuchs K, Montagnani L, Wolf S, Delpierre N, Berveiller D, Gharun M, Marchesini LB, Gianelle D, Šigut L, Mammarella I, Siebicke L, Black TA, Knohl A, Hörtnagl L, Magliulo V, Besnard S, Weber U, Carvalhais N, Migliavacca M, Reichstein M, Jung M (2020) Ecosystem transpiration and evaporation: Insights from three water flux partitioning methods across FLUXNET sites. Glob Change Biol 26:6916–6930

Papale D, Reichstein M, Aubinet M, Canfora E, Bernhofer C, Kutsch W, Longdoz B, Rambal S, Valentini R, Vesala T et al (2006) Towards a standardized processing of Net Ecosystem Exchange measured with eddy covariance technique: algorithms and uncertainty estimation. Biogeosciences 3:571–583. https://doi.org/10.5194/bg-3-571-2006

Parthasarathy B (1984) Interannual and long-term variability of Indian summer monsoon rainfall. Proc Indian Acad Sci Planet Sci 93:371–385. https://doi.org/10.1007/BF02843255

Passioura JB, Ball MC, Knight JH (1992) Mangroves may salinize the soil and in so doing limit their transpiration rate. Funct Ecol 6:476–481. https://doi.org/10.2307/2389286

Priestley CHB, Taylor RJ (1972) On the assessment of surface heat flux and evaporation using large-scale parameters. Mon Weather Rev 100:81–92. https://doi.org/10.1175/1520-0493(1972)100%3c0081:otaosh%3e2.3.co;2

Purvaja R, Ramesh R, Frenzel P (2004) Plant-mediated methane emission from an Indian mangrove. Glob Change Biol 10:1825–1834. https://doi.org/10.1111/j.1365-2486.2004.00834.x

R Development Core Team R (2011) R: A language and environment for statistical computing, R foundation for statistical computing. https://doi.org/10.1007/978-3-540-74686-7

Rajeevan M, Gadgil S, Bhate J (2010) Active and break spells of the Indian summer monsoon. J Earth Syst Sci 119:229–247. https://doi.org/10.1007/s12040-010-0019-4

Rodda SR, Thumaty KC, Jha CS, Dadhwal VK (2016) Seasonal variations of carbon dioxide, water vapor and energy fluxes in Tropical Indian Mangroves. Forests 7:35. https://doi.org/10.3390/f7020035

Roth BE, Slatton KC, Cohen MJ (2007) On the potential for high-resolution lidar to improve rainfall interception estimates in forest ecosystems. Front Ecol Environ 5:421–428. https://doi.org/10.1890/060119.01

Sarma D, Baruah KK, Chakraborty S, Karipot A, Baruah R (2019) Impact of ecosystem respiration on carbon balance in a semi-evergreen forest of Northeast India. Curr Sci 116:751–757. https://doi.org/10.18520/cs/v116/i5/751-757

Satapathy DR, Krupadam RJ, Kumar LP, Wate SR (2007) The application of satellite data for the quantification of mangrove loss and coastal management in the Godavari estuary, East Coast of India. Environ Monit Assess 134:453–469. https://doi.org/10.1007/s10661-007-9636-z

Scanlon TM, Sahu P (2008) On the correlation structure of water vapor and carbon dioxide in the atmospheric surface layer: a basis for flux partitioning. Water Resour Res 44:W10418. https://doi.org/10.1029/2008WR006932

Scanlon TM, Kustas WP (2010) Partitioning carbon dioxide and water vapor fluxes using correlation analysis. Agric for Meteorol 150:89–99. https://doi.org/10.1016/j.agrformet.2009.09.005

Scanlon TM, Kustas WP (2012) Partitioning evapotranspiration using an eddy covariance-based technique: improved assessment of soil moisture and land-atmosphere exchange dynamics. Vadose Zool J. https://doi.org/10.2136/vzj2012.0025

Scanlon TM, Schmidt DF, Skaggs TH (2019) Correlation-based flux partitioning of water vapor and carbon dioxide fluxes: Method simplification and estimation of canopy water use efficiency. Agric for Meteorol 279:107732

Schüttemeyer D, Moene AF, Holtslag AAM, de Bruin HAR, van de Giesen N (2006) Surface fluxes and characteristics of drying semi-arid terrain in West Africa. Bound-Layer Meteorol 118:583–612. https://doi.org/10.1007/s10546-005-9028-2

Sellers PJ (1987) Canopy reflectance, photosynthesis, and transpiration, II. The role of biophysics in the linearity of their interdependence. Remote Sens Environ 21:143–183. https://doi.org/10.1016/0034-4257(87)90051-4

Sellers PJ (1997) Modeling the exchanges of energy, water, and carbon between continents and the atmosphere. Science (80-) 275:502–509. https://doi.org/10.1126/science.275.5299.502

Selvam V (2003) Environmental classification of mangrove wetlands of India. Curr Sci 84:757–765

Singh SK, Srivastava PK, Gupta M, Thakur JK, Mukherjee S (2014) Appraisal of land use/land cover of mangrove forest ecosystem using support vector machine. Environ Earth Sci 71:2245–2255. https://doi.org/10.1007/s12665-013-2628-0

Sippo JZ, Lovelock CE, Santos IR, Sanders CJ, Maher DT (2018) Mangrove mortality in a changing climate: an overview. Estuar Coast Shelf Sci 215:241–249. https://doi.org/10.1016/j.ecss.2018.10.011

Skaggs TH, Anderson RG, Alfieri JG, Scanlon TM, Kustas WP (2018) Fluxpart: Open source software for partitioning carbon dioxide and water vapor fluxes. Agric for Meteorol 253–254:218–224. https://doi.org/10.1016/j.agrformet.2018.02.019

Sreejith OP, Pai DS, Mohapatra M (2018) Monsoon 2018 A Report. National ClimateCentre, India Meteorological Department, Pune, India. https://imdpune.gov.in/Clim_Pred_LRF_New/Reports/monsoon_Reports.html

Stoy PC, El-Madany TS, Fisher JB, Gentine P, Gerken T, Good SP, Klosterhalfen A, Liu S, Miralles DG, Perez-Priego O, Rigden AJ, Skaggs TH, Wohlfahrt G, Anderson RG, Coenders-Gerrits AMJ, Jung M, Maes WH, Mammarella I, Mauder M, Migliavacca M, Nelson JA, Poyatos R, Reichstein M, Scott RL, Wolf S (2019) Reviews and syntheses: turning the challenges of partitioning ecosystem evaporation and transpiration into opportunities. Biogeosciences 16:3747–3775. https://doi.org/10.5194/bg-16-3747-2019

Sulman BN, Roman DT, Scanlon TM, Wang L, Novick KA (2016) Comparing methods for partitioning a decade of carbon dioxide and water vapor fluxes in a temperate forest. Agric for Meteorol 226:229–245

Suresh R, Bhatnagar AK (2005) Seasonal variability of raindrop size distribution over Cuddalore, a coastal station in Tamilnadu of southern peninsular India. Mausam 56:643–658

Thom AS (1972) Momentum, mass and heat exchange of vegetation. Q J R Meteorol Soc 98:124–134. https://doi.org/10.1002/qj.49709841510

van Rossum G, Drake FL (2009) The Python language reference manual. Linux J. https://doi.org/10.1159/0000113495

Verheijen LM, Aerts R, Brovkin V, Cavender-Bares J, Cornelissen JHC, Kattge J, van Bodegom PM (2015) Inclusion of ecologically based trait variation in plant functional types reduces the projected land carbon sink in an earth system model. Glob Change Biol 21:3074–3086. https://doi.org/10.1111/gcb.12871

Verma SB (1987) Aerodynamic resistances to transfers of heat, mass and momentum In: Aerodynamic resistances to transfers of heat, mass and momentum. Estimation of Areal Evapotranspiration, IAHS Publication, Canada. https://scholar.google.com/scholar_lookup?title=Aerodynamic%20Resistances%20to%20Transfers%20of%20Heat%2C%20Mass%20and%20Momentum&publication_year=1989&author=S.B.%20Verma

Wang K, Dickinson RE (2012) A review of global terrestrial evapotranspiration: observation, modelling, climatology, and climatic variability. Rev Geophys 50:1–54. https://doi.org/10.1029/2011RG000373

Waskom ML (2021) seaborn: statistical data visualization. J Open Source Softw 6(60):3021. https://doi.org/10.21105/joss.03021

Wilson K et al (2002) Energy balance closure at FLUXNET sites. Agric for Meteorol 113:223–243. https://doi.org/10.1016/S0168-1923(02)00109-0

Zade M, Ray SS, Dutta S, Panigrahy S (2005) Analysis of runoff pattern for all major basins of India derived using remote sensing data. Current Sci 1301-1305.